

CANCER

Bifunctional cancer cell–based vaccine concomitantly drives direct tumor killing and antitumor immunity

Kok-Siong Chen^{1,2}, Clemens Reinshagen^{1,2}, Thijs A. Van Schaik^{1,2}, Filippo Rossignoli^{1,2}, Paulo Borges^{1,2}, Natalia Claire Mendonca^{1,2}, Reza Abdi^{3,4}, Brennan Simon^{1,2}, David A. Reardon^{4,5}, Hiroaki Wakimoto^{1,2,6}, Khalid Shah^{1,2,7*}

Copyright © 2023 The Authors, some rights reserved; exclusive licensee American Association for the Advancement of Science. No claim to original U.S. Government Works

The administration of inactivated tumor cells is known to induce a potent antitumor immune response; however, the efficacy of such an approach is limited by its inability to kill tumor cells before inducing the immune responses. Unlike inactivated tumor cells, living tumor cells have the ability to track and target tumors. Here, we developed a bifunctional whole cancer cell–based therapeutic with direct tumor killing and immunostimulatory roles. We repurposed the tumor cells from interferon- β (IFN- β) sensitive to resistant using CRISPR-Cas9 by knocking out the IFN- β -specific receptor and subsequently engineered them to release immunomodulatory agents IFN- β and granulocyte-macrophage colony-stimulating factor. These engineered therapeutic tumor cells (ThTCs) eliminated established glioblastoma tumors in mice by inducing caspase-mediated cancer cell apoptosis, down-regulating cancer-associated fibroblast-expressed platelet-derived growth factor receptor β , and activating antitumor immune cell trafficking and antigen-specific T cell activation signaling. This mechanism-based efficacy of ThTCs translated into a survival benefit and long-term immunity in primary, recurrent, and metastatic cancer models in immunocompetent and humanized mice. The incorporation of a double kill-switch comprising herpes simplex virus–1 thymidine kinase and rapamycin-activated caspase 9 in ThTCs ensured the safety of our approach. Arming naturally neoantigen-rich tumor cells with bifunctional therapeutics represents a promising cell-based immunotherapy for solid tumors and establishes a road map toward clinical translation.

INTRODUCTION

Therapeutic tumor cells (ThTCs) hold promise as anticancer agents because of their ability to serve as the natural source of neoantigens. They are typically inactivated by lysis or irradiation before being re-administered into the body to enhance immunogenicity (1–4). This approach has been shown to trigger robust immune cell trafficking to the tumor site (5–8), resulting in the induction of an antitumor immune response in different cancer types (9–13). Phase 1 to 3 clinical trials have tested the therapeutic efficacy of inactivated tumor cells for various types of cancer, including non–small cell lung carcinoma (NCT00298298), colorectal cancer (NCT00780988), melanoma (NCT01453361), and Ewing's sarcoma (NCT01061840). However, this therapeutic approach showed limited or no clinical benefit (4, 14, 15), which could be attributed to the lack of direct cytotoxic effect on tumor cells and the inability to trigger a strong antitumor immune response.

Unlike inactivated tumor cells, living tumor cells have a unique potential to home to and target tumors (16–20). Therefore, engineering tumor cells to express therapeutic agents is a rational approach that takes advantage of their natural source of

neoantigens. Among various therapeutic agents used in cancer treatment, interferon- β (IFN- β) is appealing because of its direct effects, such as inhibition of tumor cell proliferation and angiogenesis (21–26), and indirect effects, such as activation of antitumor immune responses (23). However, engineering tumor cells to stably secrete IFN- β as a self-targeted anticancer treatment is limited by premature cell death because of autocrine toxicity (25, 27, 28).

Here, we developed a bifunctional therapeutic strategy by transforming living tumor cells into a potent agent that concomitantly drives direct tumor killing and antitumor immunity. We first used CRISPR-Cas9 to knock out the IFN- β -specific receptor (IFNAR1) in inherently IFN- β -sensitive syngeneic tumor cells and subsequently engineered them to constitutively produce IFN- β for tumor cell targeting and simultaneous immunomodulation. These therapeutic cells are further designed to coexpress granulocyte-macrophage colony-stimulating factor (GM-CSF) that facilitates the differentiation, proliferation, and recruitment of dendritic cells (DCs). GM-CSF expression promotes DCs' capacity for antigen cross-presentation, costimulatory molecule expression, and proinflammatory cytokine production (29, 30), thereby priming the immune system for long-term antitumor responses (2, 31–34). To eliminate the possibility of unwanted secondary tumor initiation, we implemented a dual safety switch comprising herpes simplex virus–1 thymidine kinase (HSV-TK) and rapamycin-activated caspase 9 (RapaCasp9) in these ThTCs. We demonstrate a multimechanistic tumor cell–based therapeutic approach that can eliminate tumor cells and induce active and long-term immunity, which translates into marked survival benefits in primary, recurrent, and metastatic mouse cancer models.

¹Center for Stem Cell and Translational Immunotherapy, Brigham and Women's Hospital, Harvard Medical School, Boston, MA 02115, USA. ²Department of Neurosurgery, Brigham and Women's Hospital, Harvard Medical School, Boston, MA 02115, USA. ³Transplantation Research Center, Renal Division, Brigham and Women's Hospital, Harvard Medical School, Boston, MA 02115, USA. ⁴Department of Medicine, Brigham and Women's Hospital, Boston, MA 02115, USA. ⁵Center for Neuro-Oncology, Dana-Farber Cancer Institute, Department of Medicine, Harvard Medical School, Boston, MA 02115, USA. ⁶Department of Neurosurgery, Massachusetts General Hospital, Harvard Medical School, Boston, MA 02138, USA. ⁷Harvard Stem Cell Institute, Harvard University, Cambridge, MA 02138, USA.

*Corresponding author. Email: kshah@bwh.harvard.edu

RESULTS

Robust type I IFN signaling correlates with improved therapeutic outcome for patients with cancer and an immune-active tumor microenvironment

To understand how the regulation of type I IFN signaling within the tumor microenvironment (TME) affects the patients' clinical outcome, primary tumor samples in the Cancer Genome Atlas (TCGA) dataset were *K*-means clustered into three groups (clusters K1 to K3) based on the type I IFN signaling gene signature,

hereinafter referred to as "IFN^{reg}" (Fig. 1A and table S1). Cluster K3 was associated with the most robust IFN^{reg}, whereas K1 was associated with the least IFN^{reg} (Fig. 1B). Cluster K1 constituted the largest portion of samples across most of the cancer types, especially for brain tumors (fig. S1A and table S1). A robust IFN^{reg} as reflected by the cluster K3 subtype was associated with an improved clinical outcome and a significantly better prognosis ($P < 0.01$; fig. S1B and table S1). A similar analysis using the Chinese Glioma Genome Atlas mRNA sequencing public dataset (35) also demonstrated

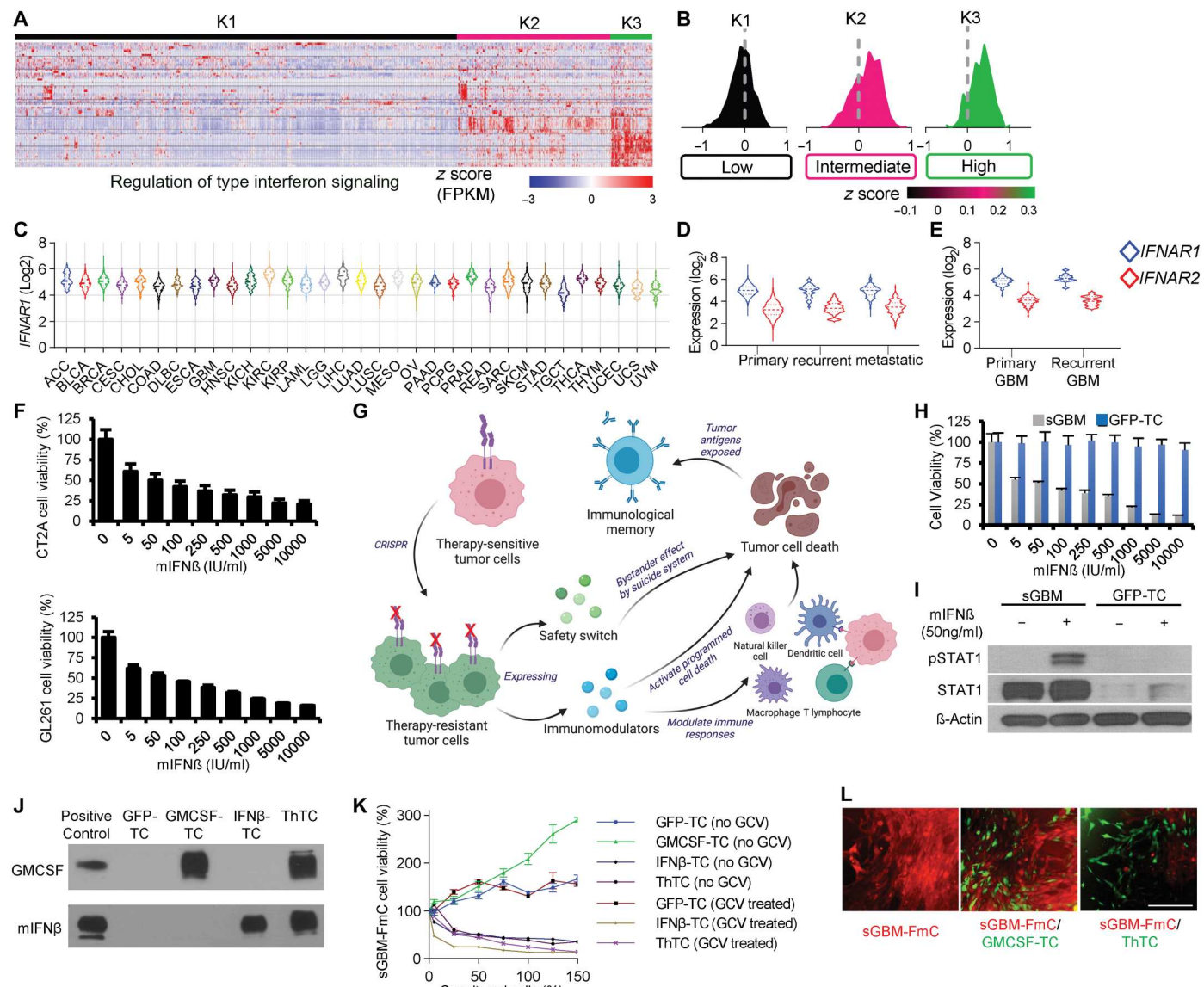


Fig. 1. Targeting type I IFN signaling within TME using CRISPR-edited and engineered ThTCs. (A) *K*-means clustering of primary tumor samples ($n = 2785$) in TCGA on the basis of IFN^{reg} (GO: 0060338) expression signature using R2 (<https://r2.amc.nl>). FPKM, fragments per kilobase of exon per million mapped fragments. (B) Distributions of IFN^{reg} signature scores within the three *K*-means clusters, with dashed line indicating the median. (C) Expression of *IFNAR1* by cancer types ($n = 10,275$). (D) Expression of *IFNAR1* and *IFNAR2* by primary ($n = 9834$), recurrent ($n = 47$), and metastatic ($n = 394$) tumor samples. (E) Expression of *IFNAR1* and *IFNAR2* by primary ($n = 156$) and recurrent ($n = 13$) GBM samples. (F) Cell viability assay of CT2A (top) and GL261 (bottom) upon treatment with recombinant mIFN- β in a dose-dependent manner. (G) A schematic showing *Ifnar1* CRISPR editing of tumor cells and further engineering to secrete IFN- β and GM-CSF, as well as a safety switch to create ThTCs. (H) Cell viability of GFP-TCs treated with recombinant mIFN- β . (I) Western blot analysis of phosphorylated STAT1 upon treatment of recombinant mIFN- β in GFP-TCs. (J) Western blot analysis of mIFN- β and GM-CSF from ThTCs. (K) Cell viability of sGBM-FmC cells cocultured with engineered TC cells, treated with or without GCV. (L) Representative fluorescence photomicrograph of sGBM-FmC cells (red) cocultured with GM-CSF-TCs (green) or cocultured with ThTCs (green). Scale bar, 200 μ m.

that cluster K3 was associated with a better probability of survival (fig. S1, C and D, and table S1). These findings suggest that stimulating type I IFN signaling activities within the TME is likely to improve therapeutic efficacy for patients with cancer.

To understand the association of type I IFN signaling and immunomodulation of the TME, we examined the gene expression of immunomodulators (IMs) in tumor samples from K1 to K3 groups on the basis of the IM signatures described previously (fig. S1E and table S1) (36). Generally, cluster K1 had the lowest immunomodulatory activity within the TME (fig. S1E). Correlation analyses demonstrated that IFN^{reg} score for all K1 to K3 samples had a moderate to strong correlation (37) with all three signature set scores (fig. S1F), indicative of the impact of the type I IFN signaling on immunomodulation within the TME. On the basis of previously described immune subtyping (36), cluster K3 tumors are associated with more immune-active subtypes (fig. S1G). In general, the K1, K2, and K3 groups had distinct immune cell distributions within the TME (fig. S1H). Upon checking the mean ratios of immune cell activation and polarization status, K3 had a higher activated-to-naïve ratio of memory B cells, memory CD4 T cells, natural killer (NK) cells, and DCs, as well as a higher M1-to-M2 ratio of macrophages, than the two other clusters (fig. S1I), highlighting the association of type I IFN signaling in shaping the more immune-active TME.

IFN- β is an ideal therapeutic agent to target immune-inert tumors

To determine whether these tumors are targetable by IFN- β , which acts as an activating cytokine in IFN signaling, we first confirmed that *IFNAR1/2* are expressed at the mRNA level with a relatively low range of variations across different types of cancer samples (Fig. 1C, fig. S1J, and table S1) and stages of progression (Fig. 1D and table S1) in a TCGA dataset ($n = 10,275$). Similarly, *IFNAR1/2* was expressed universally across different IFN^{reg} clusters (fig. S1K and table S1). Being one of the most aggressive and immunosuppressive tumor types, primary and recurrent glioblastoma (GBM) in TCGA were specifically verified to have a comparable expression of *IFNAR1/2* (Fig. 1E and table S1). Upon checking molecular subtypes of GBM, *IFNAR1/2* expression was comparable to the common markers used for determining subtypes in the bulk RNA sequencing (RNA-seq) TCGA dataset (fig. S1L and table S1) and the single-cell RNA-seq dataset (GSE57872; fig. S1M and table S1) (38). These findings imply the wide applicability of IFN- β as a therapeutic agent for direct tumor targeting and activating type I IFN signaling within the TME regardless of tumor subtype.

Generation of CRISPR-edited and engineered tumor cells to target IFN- β -sensitive tumor

Preclinical syngeneic mouse tumor models play a crucial role in testing and understanding the immune response of therapies before their clinical translation. In our recent studies, we have shown that CT2A and Mut3 syngeneic GBM tumors are relatively immunologically inert compared with GL261 and GL005 (39). Upon checking their gene expression of IMs as previously described (40) using the murine GBM dataset (GSE151414), CT2A and Mut3 had relatively low immunostimulatory and antigen presentation scores (fig. S2A and table S2). We also scored them on the basis of IFN^{reg} signature with mouse orthologs [Gene Ontology (GO): 0060338]; the immunosuppressive CT2A and Mut3 tumors had a

relatively low IFN^{reg} score (fig. S2B and table S2). Consistent with the analysis with human cancer data, type I IFN signaling robustness likely shapes the TME immune profile of these syngeneic GBM tumors.

To investigate whether the syngeneic GBM tumors are targetable by type I IFN as seen in human GBM, we first confirmed *Ifnar1/2* expression in these GBMs (fig. S2C and table S2). The IFNAR1 expression on the cell surface of CT2A was also confirmed using flow cytometry (fig. S2D). To test their sensitivity to IFN- β , we treated CT2A and GL261 cell lines with different concentrations of recombinant mouse IFN- β (mIFN- β). Cell viability of both cell lines was inhibited in a dose-dependent manner (Fig. 1F), confirming the direct cytotoxic effect of IFN- β on these GBM cell lines in vitro. Because CT2A is known to be the most aggressive and immunosuppressive syngeneic GBM cell line (39, 41, 42), we chose this as our experimental model, hereinafter referred to as immunosuppressive GBM (sGBM).

To establish a syngeneic self-targeting tumor model, we performed several steps of genetic engineering on mouse tumor cells (Fig. 1G). Specifically, to avoid autocrine toxicity, we knocked out *Ifnar1*, the most crucial subunit of the IFN- α/β receptor for signal transduction (43, 44), on sGBM cells using CRISPR-Cas9. This resulted in mIFN- β -resistant cells, hereinafter referred to as "GFP-expressing sGBM tumor cells (GFP-TCs)" because of simultaneous labeling with GFP (green fluorescent protein). Genomic DNA of *Ifnar1* knockout GFP-TCs was confirmed by Sanger sequencing, where an indel mutation was detected at exon 2 of *Ifnar1* (fig. S2E). To verify resistance, we treated GFP-TCs with recombinant mIFN- β , which did not reduce cell viability regardless of the concentration of mIFN- β tested (Fig. 1H). Moreover, no phosphorylation of signal transducer and activator of transcription 1 (STAT1) was observed according to Western blot analysis on cell lysates (Fig. 1I), confirming a reduction of Janus kinase-STAT signaling activation as a result of *Ifnar1* knockout. To enable cell killing and immunomodulatory effects, we engineered IFN- β -resistant GFP-TC cells to secrete mIFN- β integrated with the suicide gene the HSV-TK, hereinafter referred to as "mIFN- β -expressing sGBM tumor cells (IFN- β -TC)." For additional long-term immunity priming effects, IFN- β -TCs were further engineered to secrete GM-CSF, hereinafter referred to as "ThTCs." As a control, IFN- β -resistant GFP-TCs were also engineered to secrete GM-CSF only, hereinafter referred to as "GM-CSF-expressing sGBM tumor cells (GMCSF-TCs)." The secretion of mIFN- β and GM-CSF was validated with Western blot analysis using the conditioned medium collected from the culture of engineered cells (Fig. 1J and fig. S2F). The suicide system of HSV-TK in ThTCs was confirmed, where ganciclovir (GCV) treatment induced cell death for ThTCs in a dose-dependent manner (fig. S2G).

ThTCs inhibit tumor growth in vitro

Cocultures of GFP-TCs, GMCSF-TCs, IFN- β -TCs, and ThTCs with the parental sGBM engineered with a lentivirus expressing firefly luciferase (Fluc)-mCherry, hereinafter referred to as "sGBM-FmC," showed that whereas no cytotoxic effect was observed in coculture of GFP-TCs with sGBM-FmC, robust cell killing over time was seen with coculture of IFN- β -TCs and ThTCs (Fig. 1, K and L). These cell cytotoxic effects of IFN- β -TCs and ThTCs were enhanced after GCV treatment because of bystander effects, because this effect was not observed for GFP-TCs (Fig. 1K). In contrast,

increased cell proliferation was observed for the coculture of GM-CSF-TCs with sGBM-FmC (Fig. 1, K and L). To confirm that cell cytotoxicity was mediated by mIFN- β secreted from the engineered cells, we observed no cytotoxic effect in coculture of GFP-TCs and IFN- β -TCs with mIFN- β -resistant GFP-TC-FmC, whereas increased cell proliferation was observed for both GMCSF-TCs and ThTCs in coculture with mIFN- β -resistant GFP-TC-FmC (fig. S2H). Together, these findings indicate that tumor cells can be CRISPR-edited and engineered to express IFN- β for executing self-targeting cytotoxic effects on parental tumor cells without autocrine toxicity.

ThTCs inhibit tumor growth and induce a long-term immunity mediated by T cells in vivo

To determine the effect of the engineered tumor cells on tumor growth in vivo, we performed intracranial implantation of sGBM-FmC, GFP-TC-FmC, GMCSF-TC-FmC, IFN- β -TC-FmC, and ThTC-FmC in immunocompetent C57BL/6 mice (Fig. 2A). bioluminescent Fluc imaging (BLI) revealed aggressive tumor growth for all mice implanted with sGBM-FmC (Fig. 2B and fig. S3A) and GFP-TC-FmC (Fig. 2B and fig. S3B). For GMCSF-TC-FmC, 5 of 10 mice had observable tumors (Fig. 2B and fig. S3C), implying that GM-CSF secretion reduced the likelihood of tumor growth. On the other hand, for IFN- β -TC-FmC, only 2 of 12 mice had tumors (Fig. 2B and fig. S3D), indicating a stronger inhibition of tumor growth by mIFN- β than GM-CSF. None of the mice implanted with ThTC-FmC had tumor growth (Fig. 2B and fig. S3E), and all of the mice from this group had a significantly better survival outcome compared with those in other groups ($P < 0.001$; Fig. 2C), suggesting that mIFN- β and GM-CSF functioned additively to inhibit tumor growth and improve mouse survival. Similar studies performed in male C57BL/6 mice revealed that the ThTCs are effective in improving survival regardless of sex (fig. S3, F and G).

To test the vaccine effects of ThTCs, we next rechallenged the mice surviving from the first implantation after 2 months with the parental sGBM-FmC cells in the contralateral brain hemisphere (Fig. 2A). No tumor growth was observed in 2 of 5 mice from the GMCSF-TC-FmC group (Fig. 2D and fig. S3H), 8 of 10 mice from the IFN- β -TC-FmC group (Fig. 2D and fig. S3I), and all mice from the ThTC group (Fig. 2D and fig. S3J). These tumor-free mice survived until the termination of the experiment (Fig. 2E). These findings indicate that the engineered tumor cells, especially those that secrete both mIFN- β and GM-CSF, can induce long-term antitumor immunity in mice.

To investigate whether tumor growth inhibition is mediated by a specific subset of immune cells, we used severe combined immunodeficiency (SCID) mice that are T cell and B cell deficient but have intact NK cells, DCs, and macrophages (45). Tumors were observed in all mice implanted with ThTC-FmC (Fig. 2F), suggesting that the function of mIFN- β and GM-CSF in inhibiting tumor growth requires either T cells or B cells. The efficacy of the HSV-TK suicide system was also tested in vivo in the same experiment, where two of the tumor-bearing mice were treated with GCV daily starting from day 8 after implantation (Fig. 2F), and the Fluc signal decreased markedly as compared with tumor-bearing mice without GCV treatment (Fig. 2, F and G), indicating that the ThTC-FmC cells were successfully eradicated upon GCV treatment.

To further delineate whether T cells or B cells are responsible for inhibiting tumor growth, we used athymic nude mice, which are T cell-deficient but with intact B cells, NK cells, DCs, and macrophages (46). Similar to SCID mice, tumors were observed in all nude mice implanted with ThTC-FmC (fig. S3K), suggesting that T cells are crucial to inhibit tumor growth. Moreover, the median survival for both tumor-bearing SCID and nude mice was 22 days after implantation (Fig. 2G), which was consistent with the median survival of C57BL/6 mice implanted with sGBM-FmC cells (Fig. 2C). This confirmed that tumor growth rate of the gene-edited and gene-engineered tumor cells is comparable to unmodified cells if T cells were absent.

To confirm the specific subtype of T cells that is responsible for tumor growth inhibition, we performed T cell depletion in C57BL/6 mice before and after the implantation with ThTC-FmC cells (Fig. 2H). The depletion of CD4⁺ cells, CD8⁺ cells, or both in the brain was confirmed with immunofluorescent staining (Fig. 2H). No tumors were observed in mice without antibody treatment or in mice treated with either CD4 antibody or CD8 antibody (Fig. 2J). On the other hand, tumor growth was observed in all mice treated with both CD4 and CD8 antibodies (Fig. 2J), and the median survival of these tumor-bearing mice was 30 days (Fig. 2K). These findings imply that both CD4⁺ and CD8⁺ T cells contributed to the antitumor response seen in immune-intact mice implanted with ThTC-FmC cells.

To determine whether depletion of either CD4⁺ or CD8⁺ cells during the first tumor implantation influences the immunological memory driven by ThTC-FmC as seen in Fig. 2E, we rechallenged the surviving mice from groups treated with either CD4 antibody or CD8 antibody with the parental sGBM-FmC (Fig. 2I). Tumor growth was observed in all mice treated with CD4 antibody during the first implantation compared with one of three mice treated with CD8 antibody (Fig. 2, L and M). These findings suggest that the immunological memory effect of ThTCs is mediated mainly by CD4⁺ T cells.

ThTCs eradicate residual tumor cells at the resection cavity and prevent recurrence

To assess the therapeutic impact of the ThTCs in a clinically relevant context, established tumors were resected, and engineered tumor cells encapsulated with nonimmunogenic hyaluronic acid-based synthetic extracellular matrix (sECM) were administered into the resection cavity as treatment (Fig. 3A). Tumors recurred, and the animals had to be euthanized 10 days after treatment in the sECM-only, GFP-TC, GMCSF-TC, and IFN- β -TC groups, whereas residual tumor cells at the cavity were completely eradicated in 10 of 12 mice 8 days after treatment for the ThTC group (Fig. 3, B and C). The median survival for the ThTC group was significantly improved compared with the control groups ($P < 0.01$; Fig. 3D). A higher number of cleaved-Caspase3, denoting apoptotic cells, was observed in tumor tissues treated with ThTCs compared with sECM-only and GFP-TC groups based on immunofluorescence staining analysis (Fig. 3, E and F). This indicated higher apoptosis induction in tumors treated with ThTCs. We repeated the same experiment using immunodeficient nonobese diabetic (NOD) SCID mice, and a higher number of apoptotic cells was observed in tumors treated with ThTCs (fig. S4, A and B), confirming the direct cytotoxic effect of ThTCs to the tumor, independent from the immune response. We also performed an in vitro immune cell

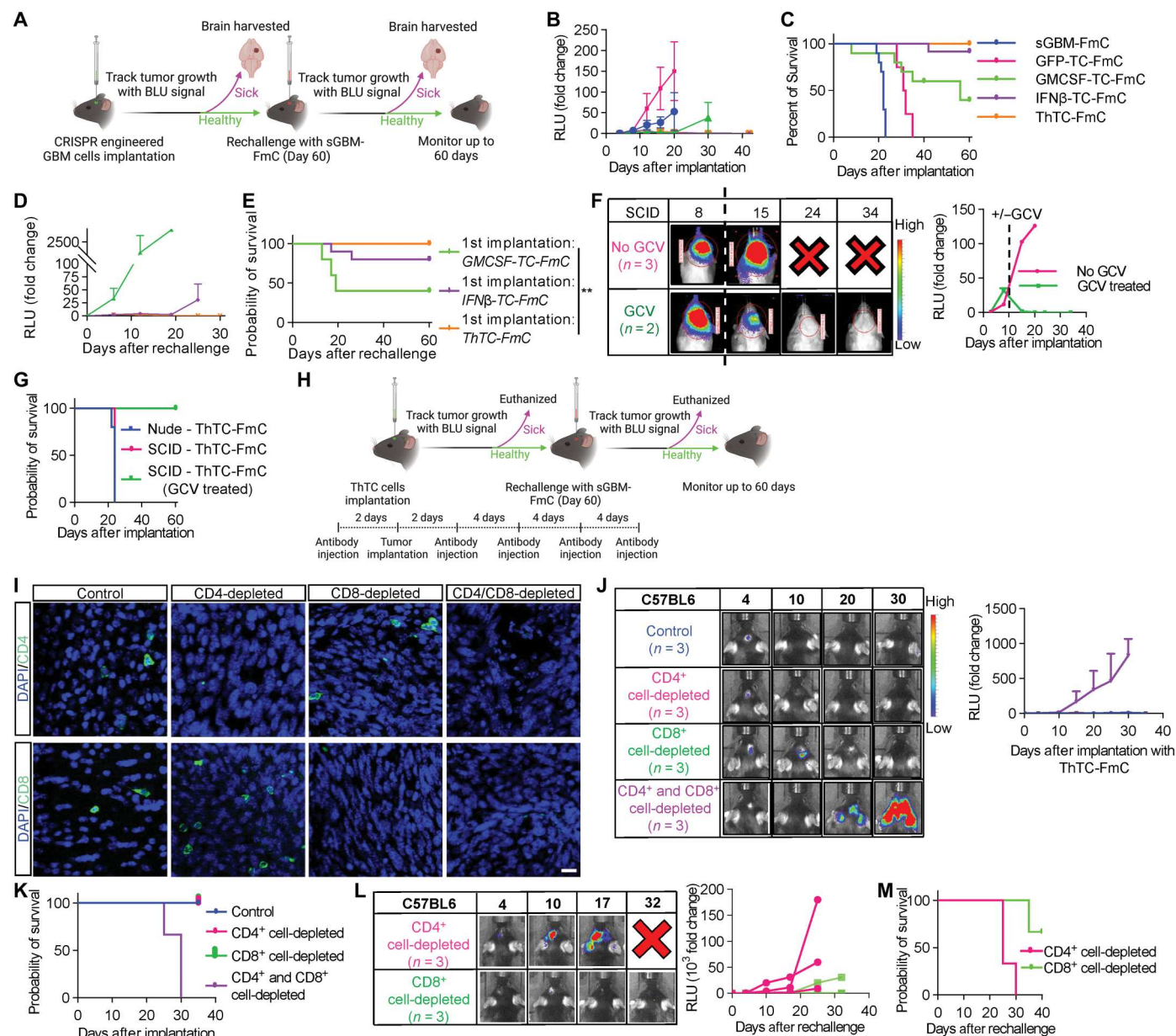


Fig. 2. ThTCs inhibit tumor growth and induce long-term immunity through T cells. (A) Schematic of the experimental timeline for intracranial GBM implantation. BLU, bioluminescence. (B) Graph of Fluc signal in C57BL/6 mice after intracranial implantation with wild-type sGBM-FmC ($n = 10$), GFP-TC-FmC ($n = 4$), GM-CSF-TC-FmC ($n = 10$), IFN- β -TC-FmC ($n = 12$), and ThTC-FmC ($n = 18$); bars represent SEMs. RLU, relative luminescence unit. (C) Kaplan-Meier curves demonstrating the survival probability of the C57BL/6 mice implanted with different cells. Log-rank (Mantel-Cox) test and Bonferroni correction. $P < 0.0001$ for sGBM-FmC versus IFN- β -TC-FmC, sGBM-FmC versus ThTC-FmC, GFP-TC-FmC versus IFN- β -TC-FmC, and GFP-TC-FmC versus ThTC-FmC. $P < 0.001$ for sGBM-FmC versus GM-CSF-TC-FmC and GM-CSF-TC-FmC versus ThTC-FmC. (D) Graph of Fluc signal in C57BL/6 mice that survived the first intracranial implantation with GM-CSF-TC-FmC ($n = 5$), IFN- β -TC-FmC ($n = 10$), and ThTC-FmC ($n = 12$) after rechallenge with sGBM-FmC cells in the contralateral brain hemisphere. (E) Kaplan-Meier curves demonstrating survival probability of C57BL/6 mice after rechallenge. Log-rank (Mantel-Cox) test and Bonferroni correction. $^{**}P < 0.01$. (F) Representative images (left) and graph (right) of Fluc signal in SCID mice treated with or without GCV after intracranial implantation with ThTC-FmCs. (G) Kaplan-Meier curves demonstrating the median survival of both SCID and nude mice implanted with ThTC-FmC with and without GCV treatment. (H) Schematic of the experimental timeline for intracranial GBM implantation with antibody injection. (I) Representative immunofluorescence staining images stained for CD4 and CD8 $^{+}$ cells in brain tumor tissues. Scale bar, 10 μ m. (J) Representative images (left) and graph (right) of Fluc signal in the C57BL/6 mice treated with CD4, CD8, CD4, and CD8 antibodies or without antibodies after intracranial implantation with ThTC-FmC cells. (K) Kaplan-Meier curves demonstrating survival probability of mice with T cell depletion. $P < 0.05$ for control versus CD4 $^{+}$ cell-depleted, control versus CD8 $^{+}$ cell-depleted, and control versus CD4 $^{+}$ and CD8 $^{+}$ cell-depleted after analysis by log-rank (Mantel-Cox) test without multiple comparisons correction. (L) Representative images (left) and graph (right) of Fluc signal from surviving C57BL/6 mice after the first intracranial implantation with the depletion of CD4 $^{+}$ or CD8 $^{+}$ cells after rechallenge with sGBM-FmC cell in the contralateral brain hemisphere. (M) Kaplan-Meier curves demonstrating survival probability of C57BL/6 mice after rechallenge.

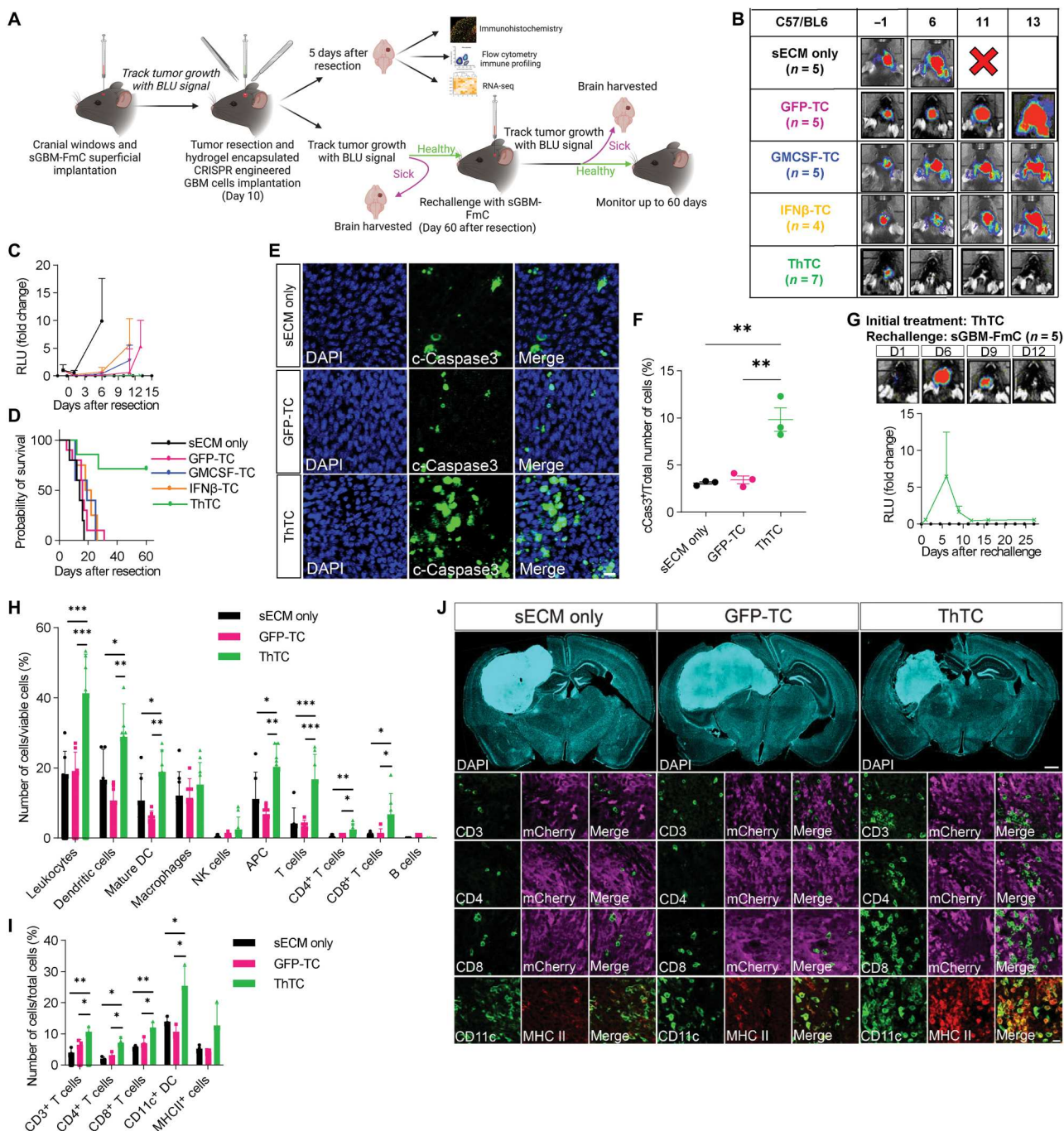


Fig. 3. ThTCs eradicate residual tumor cells in the resection cavity and prevent recurrence by recruitment of antitumor immune cells. (A) Schematic of the experimental timeline for a GBM resection model. (B) Representative images of Fluc signal from sGBM-FmC-bearing C57BL/6 mice after resection and treated with either sECM only, GFP-TCs, GMCSF-TCs, IFN β -TCs, or ThTCs. (C) Graphs of Fluc signal in sGBM-FmC-bearing C57BL/6 mice after resection and treated with either sECM only, GFP-TCs, GMCSF-TCs, IFN β -TCs, or ThTCs. (D) Kaplan-Meier curves showing survival of mice treated with ThTCs (green line) and other cells. $P < 0.01$ for sECM only versus ThTC, GFP-TC versus ThTC, GM-CSF-TC versus ThTC, and IFN β -TC versus ThTC after analysis by log-rank (Mantel-Cox) test and Bonferroni correction. (E) Representative immunofluorescence staining images showing c-Caspase3 $^{+}$ cells in the resection cavities of C57BL/6 mice. Scale bar, 10 μ m. (F) Quantification of the number of c-Caspase3 $^{+}$ cells in the resection cavities of C57BL/6 mice using the immunofluorescence images. Data were analyzed by ANOVA with Holm-Sidak test for multiple comparisons correction. $^{**}P < 0.01$. (G) Representative images (top) and graph of Fluc signal in the surviving mice shown in (D) after rechallenge with sGBM-FmC cells. (H) Bar chart showing immune profiling of tumor tissues harvested from the mouse brain 5 days after resection and treatment with sECM only, GFP-TCs, and ThTCs from three independent experiments. Data were analyzed by ANOVA with Holm-Sidak test for multiple comparisons correction. $^{*}P < 0.05$, $^{**}P < 0.01$, and $^{***}P < 0.001$. (I) Bar chart showing cell quantification of tumor tissues harvested from mouse brain 5 days after resection and treatment with sECM only, GFP-TCs, and ThTCs ($n = 3$ per group) based on immunofluorescence staining. Data were analyzed by ANOVA with Holm-Sidak test for multiple comparisons correction. $^{*}P < 0.05$ and $^{**}P < 0.01$. (J) Representative images of immunofluorescence staining of tumor tissues harvested from the mouse brain 5 days after resection and treatment. Scale bars, 500 μ m (top) and 10 μ m (bottom).

toxicity assay by treating the immune cells harvested from mouse spleens with fresh medium or conditioned medium collected from GFP-TC or ThTCs. No direct toxicity was observed on immune cells (fig. S4C). To determine whether these therapeutic cells are able to induce long-term immunity in the mice after eradication of residual tumor cells in the cavity, we rechallenged the surviving mice (Fig. 3A) by implanting sGBM-FmC cells in the contralateral brain. No tumor growth was observed for these mice (Fig. 3G). These findings suggest that ThTCs can effectively eliminate residual tumor cells and induce adaptive immunity in mice.

ThTCs recruit immune cells and activate antitumor immune responses in the resection cavity

To further clarify the immunomodulatory effect of ThTCs in this resection model, we immuno-profiled tumor tissues harvested 5 days after treatment using multicolor flow cytometry (Fig. 3A, fig. S5, and table S3). Compared with the sECM-only and GFP-TC groups, treatment with encapsulated ThTCs after treatment significantly enhanced infiltration of leukocytes ($CD45^+$, $P < 0.001$), DCs ($CD45^+/CD11c^+$, $P < 0.05$), and T cells ($CD45^+/CD3^+$, $P < 0.001$) (Fig. 3H). These findings were confirmed by quantification of $CD3^+$ and $CD11c^+$ (Fig. 3I) cells from tumor tissues using immunofluorescent staining (Fig. 3J). In addition, higher numbers of mature DCs [$CD45^+/CD11c^+$ /major histocompatibility complex (MHC) class II⁺], antigen-presenting cells (APCs; $CD45^+$ /MHC class II⁺), and $CD4^+/CD8^+$ T cells were also observed in the ThTC group compared with the sECM-only and GFP-TC groups (Fig. 3I). These results were validated with immunofluorescent staining (Fig. 3, I and J), suggesting an elevated neoantigen presentation activity induced by ThTCs.

ThTCs promote type I IFN signaling and reshape the TME to a more pronounced antitumor condition

To further elucidate the immune responses elicited by ThTCs in the resection model, we sequenced RNA extracted from tumor tissues harvested 5 days after treatment (Fig. 3A). The high correlation coefficient in sample correlation analyses (fig. S6A) and less than 50% of the variance for PC1/PC2 in principal components analyses (fig. S6B) demonstrated that the samples from these three groups were highly correlated, with low intergroup variability (47). However, a comparison of the IFN^{reg} signature expression showed that tumor tissues treated with ThTCs had significantly higher type I IFN signaling activity than the sECM-only group ($P < 0.01$, Wilcoxon test) and the GFP-TC group ($P < 0.05$, Wilcoxon test) (Fig. 4A and table S4). Moreover, the IM gene expression of tissues treated with ThTCs was relatively higher, especially for immunostimulatory and antigen presentation genes as compared with the other groups (Fig. 4B and table S4), indicating relatively more pronounced immune activity within the TME. A comparison of the expression of immune cell type-annotated genes as previously described (39, 48) showed that ThTC samples were enriched in immune cells, including T cells, macrophages, and activated DCs (Fig. 4C), corroborating the recruitment of immune cells and DC activation by ThTCs.

To characterize the immune-related pathways that were mediated by ThTCs, we performed gene set enrichment analysis (GSEA) using GO biological processes and Kyoto Encyclopedia of Genes and Genomes (KEGG) databases. Compared with sECM-only and GFP-TC groups, genes in multiple immune-related GO pathways were up-regulated by the ThTC group, including cellular response

to IFN- β , adaptive immune response, defense response, and positive regulation of NK cell-mediated cytotoxicity (Fig. 4D and table S5). On the basis of KEGG, gene sets in NK cell-mediated cytotoxicity and antigen processing and presentation were up-regulated in the ThTC group compared with sECM-only and GFP-TC groups (fig. S6C and table S6). These pathways were related to immune responses mediated by IFN- β and GM-CSF, implying that antitumor immune responses were induced by ThTCs.

On the other hand, GSEA revealed that cell cycle-related GO pathways, such as chromatin organization and DNA repair, were significantly down-regulated in the ThTC group compared with the sECM-only group (adjusted $P < 0.05$) and GFP-TC group (adjusted $P < 0.05$) (Fig. 4D and table S5). According to KEGG, gene sets in cell growth-related pathways such as transforming growth factor- β (TGF- β) signaling, Hedgehog signaling, and Notch signaling were down-regulated in the ThTC group compared with sECM-only and GFP-TC groups (fig. S6C and table S6). Down-regulation of cell cycle and cell growth signaling might reflect direct antitumor responses induced by ThTCs in our resection model.

In addition, pairwise differential gene expression analysis revealed 105 differentially expressed genes (DEGs; 63 up-regulated and 42 down-regulated) in the ThTC group when compared with the sECM-only group [Fig. 4E (left) and table S7]. The up-regulated DEGs exhibited enrichment of immune-related pathways, including cellular response to IFN- β , immune system process, innate immune response, and antigen processing and presentation (table S7), consistent with the activation of immune responses induced by ThTCs to the tumor. For down-regulated DEGs, enrichment of cell proliferation, migration, and differentiation was observed (table S7), suggesting the possible inhibition of tumor growth by ThTCs. On the other hand, 13 DEGs (11 up-regulated and 2 down-regulated) were identified in the ThTC group when compared with the GFP-TC group [Fig. 4E (right) and table S7]. Similarly, up-regulated DEGs demonstrated enrichment of immune-related pathways, such as immune response-regulating signaling pathway, neutrophil activation involved in immune response, and antigen processing and presentation of exogenous antigens (table S7). For down-regulated DEGs, enrichment of cell proliferation, migration, and differentiation was observed on the basis of GO.

Among identified DEGs in the ThTC group when compared with the sECM-only or GFP-TC groups, five were commonly up-regulated (*Tyrobp*, *Psme2*, *Ifi27l2a*, *Ms4a6b*, and *Ms4a4c*) and two were commonly down-regulated (*Notch3* and *Pdgfrb*) in the ThTC group (Fig. 4E and fig. S6D). These commonly up-regulated genes were involved in immune responses, whereas those commonly down-regulated were oncogenes involved in glioma cell proliferation. Quantitative polymerase chain reaction (qPCR) analysis validated that *Pdgfrb* was significantly down-regulated ($P < 0.05$) and that *Ifi27l2a* was significantly up-regulated ($P < 0.05$) in the ThTC group (fig. S6E). Given that *Pdgfrb* is one of the main markers for cancer-associated fibroblasts (CAFs), the therapeutic effects of ThTCs might involve CAFs. Lower expression of CAF markers was observed in all ThTC-treated tumor samples based on an unsupervised hierarchical clustering using the RNA-seq data (Fig. 4F). In addition, down-regulation of platelet-derived growth factor receptor β (PDGFRB) at the protein level for tissues treated with ThTCs was observed using immunofluorescence. However, this was not the case in other groups (Fig. 4, G and H), corroborating that the down-regulation of PDGFRB is an additive effect of both GM-CSF and

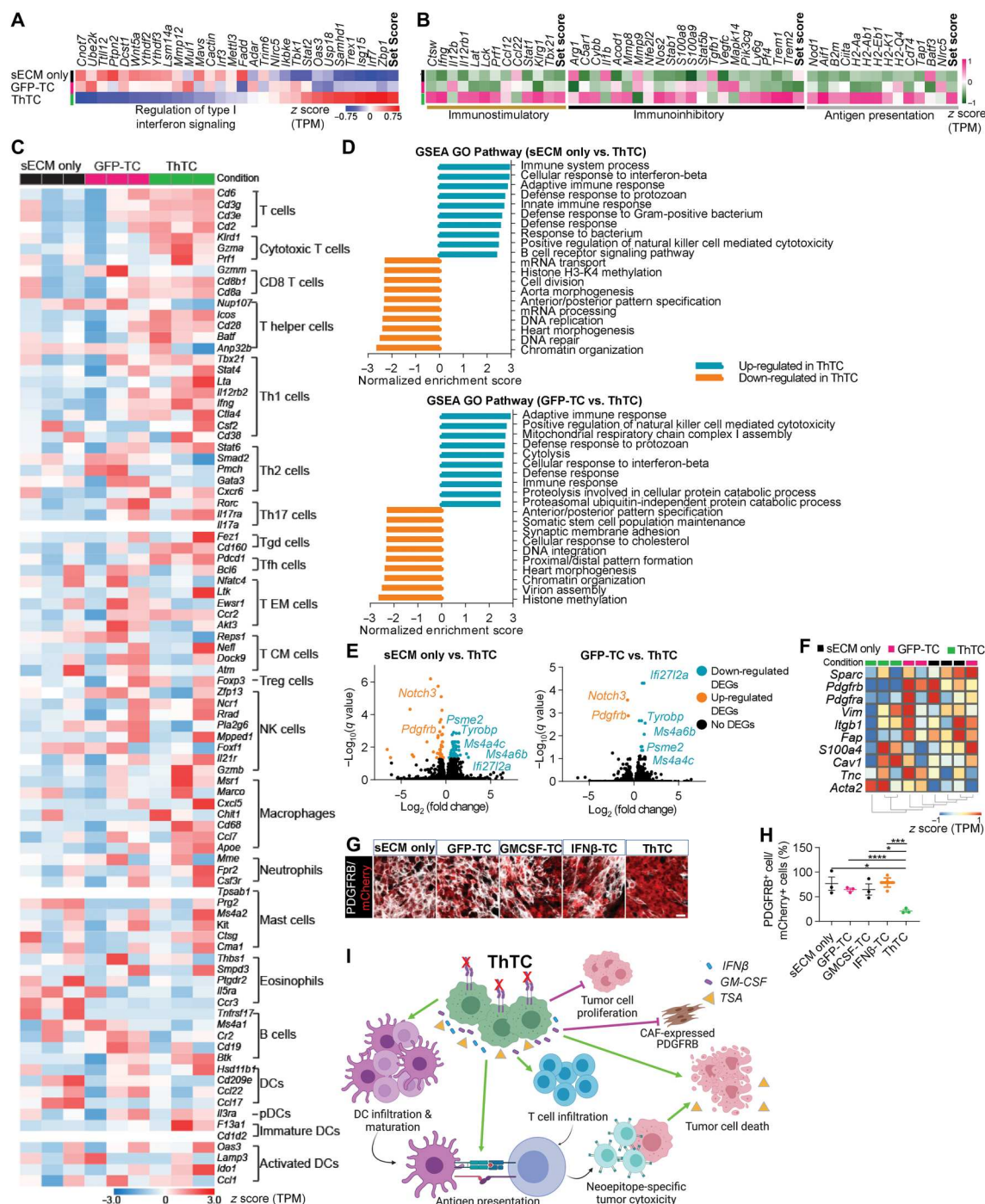


Fig. 4. ThTCs reshape the TME to a more pronounced antitumor condition and down-regulate CAF-secreted PDGFRB. (A) mRNA expression based on IFN^{reg} (GO: 0060338) signature on RNA-seq data of tumor tissues harvested from the mouse brain after resection and treatment with sECM only, GFP-TCs, and ThTCs ($n = 3$ per group). TPM, transcripts per million. (B) mRNA expression for 46 immunomodulation genes in tumor tissues harvested from the mouse brain after resection and treatment with sECM only, GFP-TCs, and ThTCs. (C) Heatmap of expression of genes associated with immune cell types in tumor tissues harvested from the mouse brain after resection and treatment with sECM only, GFP-TCs, and ThTCs, plotted as z score of normalized gene expression for each gene. (D) GSEAs demonstrating the significantly up-regulated and down-regulated GO pathways in the ThTC group compared with sECM-only group (top) or GFP-TC group (bottom). (E) Volcano plots demonstrating the up-regulated and down-regulated differentially expressed genes (DEGs) in the ThTC group when compared with the sECM-only group or the GFP-TC group. (F) Unsupervised hierarchical clustering heatmap of cancer-associated fibroblast (CAF) markers in tumor tissues harvested from the mouse brain after resection and treatment with sECM only, GFP-TCs, and ThTCs, plotted as z score of normalized gene expression. (G) Representative images of immunofluorescence staining of PDGFRB and mCherry from tumor tissues harvested from mouse brains 5 days after resection and treatment. Scale bar, 10 μm . (H) Quantification of the expression of PDGFRB in the resection cavity using the immunofluorescence images. Scale bar, 10 μm . Data were analyzed by ANOVA with Holm-Sidak test for multiple comparisons correction. $*P < 0.05$, $**P < 0.01$, and $***P < 0.001$. (I) A schematic of the putative mechanisms underlying direct and indirect antitumor effects of ThTCs.

IFN- β . GSEAs comparing the sECM or GFP-TC to the ThTC also demonstrated that the downstream signaling associated with CAFs, including TGF- β signaling, Hedgehog signaling, and Notch signaling, was down-regulated in the ThTC group (table S6). In addition, cluster K3 (high IFN^{TC} signature) had significantly lower *PDGFRB* expression in human cancer samples ($P < 0.0001$; fig. S6F and table S1), implying that high type I IFN signaling activity is conversely associated with *PDGFRB* expression in human cancer.

Given that ThTCs were able to activate CD4⁺ T cell-induced tumor cytotoxicity as shown in Fig. 2J, we asked whether the same effect could be observed in a resection model. Upon checking the transcriptomic signature (49) for tumor-specific cytotoxic CD4⁺ T cells, the TME of ThTC-treated group had significantly elevated expression compared with control sECM-only ($P < 0.01$, Wilcoxon test) or GFP-TC groups ($P < 0.01$, Wilcoxon test) (fig. S6G). In

addition, the ThTC treatment group also had significantly higher expression of the common surface biomarkers (50–54) and upstream inducers (53, 55, 56) for cytotoxic CD4⁺ T cells than sECM-only ($P < 0.05$, Wilcoxon test) and GFP-TC groups ($P < 0.01$, Wilcoxon test) (fig. S6H). These data further suggest that cytotoxic CD4⁺ T cells also contributed to the tumor elimination elicited by ThTCs in the resection cavity.

Together, findings from flow cytometry immune profiling and RNA-seq data suggest that ThTCs can directly kill residual tumor cells after treatment using caspase-mediated apoptosis and induce antitumor responses by recruiting immune cells into the tumor and promoting antigen-presenting activities. Furthermore, ThTCs down-regulated CAF-secreted *PDGFRB*. All these antitumor activities led to tumor eradication and immunological memory (Fig. 4I).

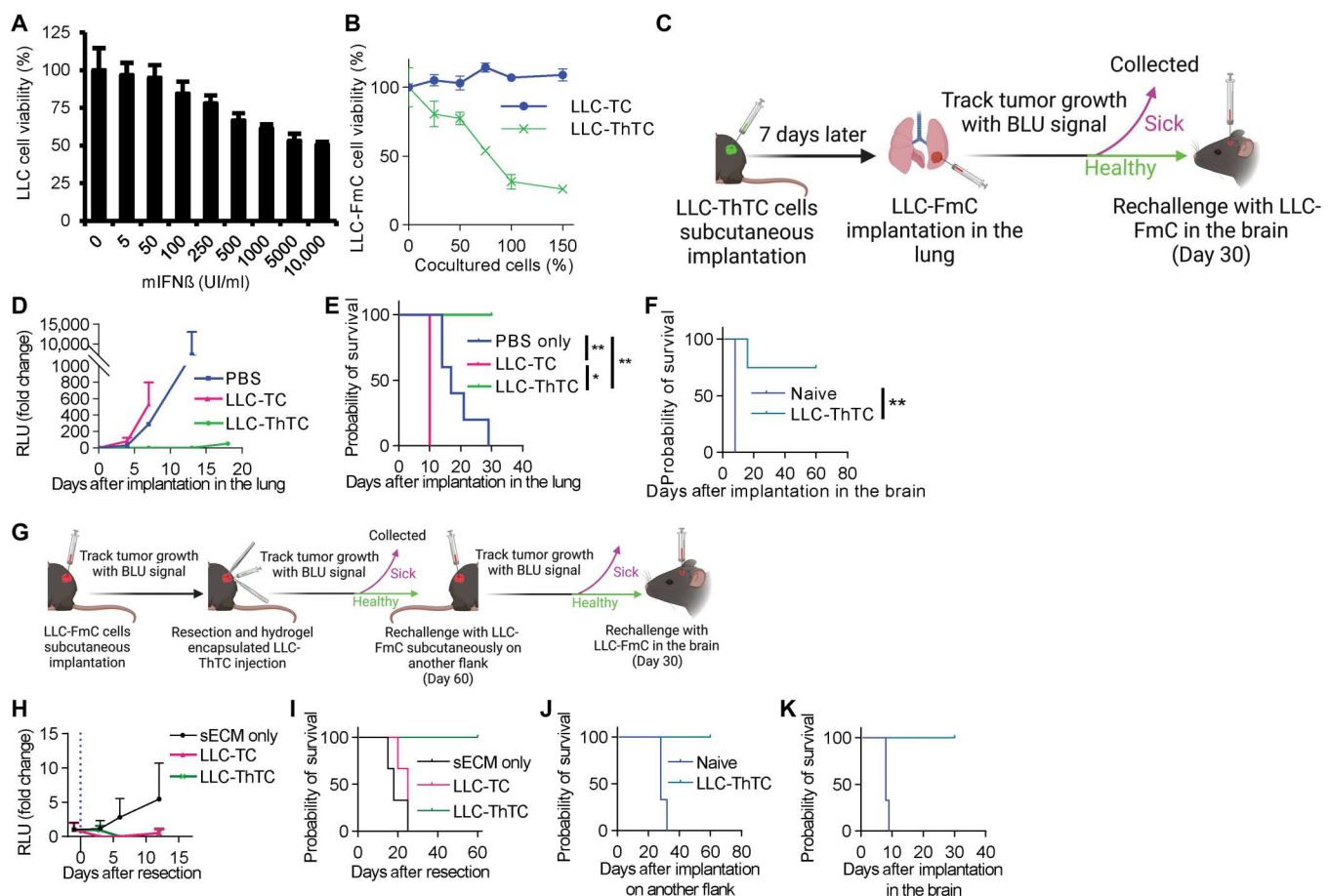


Fig. 5. Engineered GM-CSF/IFN- β -secreting tumor cells from lung cancer inhibit tumor growth and prevent distant metastasis. (A) Cell viability assay for LLC treated with increasing concentrations of recombinant mIFN- β . (B) Cell viability of coculture of parental LLC-FmC cells with LLC-TCs or LLC-ThTCs. (C) Schematic of experimental timeline of the lung tumor and distant metastasis model. (D) Fluc signal over time in the LLC-FmC-bearing C57BL/6 mice after tumor implantation in the lung with LLC-FmC cells. PBS group ($n = 5$), LLC-TC group ($n = 3$), and LLC-ThTC group ($n = 4$). (E) Kaplan-Meier curves demonstrating the survival probability of C57BL/6 mice after tumor implantation in the lung with LLC-FmC cells. Log-rank (Mantel-Cox) test and Bonferroni correction. $*P < 0.05$ and $**P < 0.01$. (F) Kaplan-Meier curves demonstrating the survival probability of C57BL/6 mice after rechallenge in the brain with LLC-FmC cells. Log-rank (Mantel-Cox) test. $**P < 0.01$. (G) Schematic of experimental timeline of lung tumor resection and distant metastasis models. (H) Fluc signal over time in LLC-FmC-bearing C57BL/6 mice after resection and treatment with either sECM only ($n = 3$), LLC-TCs ($n = 3$), or LLC-ThTCs ($n = 4$). (I) Kaplan-Meier curves demonstrating the survival probability of the C57BL/6 mice after resection and treatment. Log-rank (Mantel-Cox) test and Bonferroni correction. $P < 0.05$ for sECM only versus LLC-ThTC and LLC-TC versus LLC-ThTC. (J) Kaplan-Meier curves demonstrating the survival probability of the naïve C57BL/6 mice ($n = 3$) and surviving mice from LLC-ThTC group ($n = 4$) from (H) after rechallenge on the right flank with LLC-FmC cells. Log-rank (Mantel-Cox) test and Bonferroni correction. $P < 0.01$. (K) Kaplan-Meier curves demonstrating the survival probability of the naïve C57BL/6 mice ($n = 3$) and surviving mice from LLC-ThTC group ($n = 4$) from (J) after rechallenge in the brain with LLC-FmC cells. Log-rank (Mantel-Cox) test and Bonferroni correction. $P < 0.01$.

ThTCs exhibit therapeutic efficacy in a recurrent GBM model

Given that temozolomide (TMZ) therapy, which is commonly initiated after first-time tumor surgery, may alter sensitivity to our therapeutic approaches, a TMZ-resistant recurrent GBM (rGBM) line was established from sGBM-FmC (fig. S7A). BLI revealed a slight reduction of the tumor growth rate of TMZ-treated mice compared with mice without TMZ treatment (fig. S7B). However, tumors continued to grow despite TMZ treatment, suggesting the development of TMZ resistance. TMZ treatment improved survival of these tumor-bearing mice due to a slower tumor growth rate ($P < 0.01$; fig. S7C). When these TMZ-treated mice reached the clinical end point, tumor tissues were harvested and dissociated for cell culture as a TMZ-resistant rGBM line (hereinafter referred to as "rGBM-FmC"). qPCR analysis confirmed that the expression of genes related to TMZ resistance (*Mgmt*), DNA mismatch repair (*Mlh1*, *Msh2*, and *Msh6*), apoptosis inhibition (*Birc3* and *Klf8*), cell cycle regulation (*Igfbp2*), and cell proliferation (mKi67) was significantly higher in rGBM-FmC cells compared with sGBM-FmC ($P < 0.05$; fig. S7D), recapitulating the characteristics of rGBM cells (57).

Assessing the therapeutic impact of ThTCs in a resection GBM model using rGBM cells (fig. S7E) demonstrated that tumors recurred and animals had to be euthanized 10 days after treatment for the GFP-TC and sECM-only groups, whereas residual tumor cells in the cavity were completely eradicated in five of seven mice for the ThTC group (fig. S7F). The median survival for the ThTC group was significantly improved compared with the other groups ($P < 0.05$; fig. S7G). These findings suggest that ThTCs can effectively target chemoresistant recurrent tumor cells to prevent relapse.

Engineered GM-CSF/IFN- β -secreting tumor vaccines derived from other tumor types inhibit tumor growth and prevent distant metastasis

To determine whether this engineered cancer cell-based therapeutic approach can be applied to other tumor types, we first confirmed the sensitivity of Lewis lung carcinoma (LLC) and melanoma B16 cells to recombinant mIFN- β treatment in vitro (Fig. 5A and fig. S8A). We then generated mIFN- β -resistant LLC-TCs and B16-TCs as well as therapeutic LLC-ThTC and B16-ThTCs using similar genetic engineering steps as with sGBM (Fig. 1G). Consistent with the findings for GBM, no cytotoxicity effect was observed in coculture of LLC-TCs with LLC-FmC, but cell killing was seen for LLC-ThTCs (Fig. 5B), demonstrating the cytotoxic effect of the mIFN- β -expressing LLC tumor cells. Although not as robust, similar cell cytotoxicity of B16-ThTC was observed when cocultured with B16-FmC, whereas no cytotoxic effect was noted for B16-TC (fig. S8B).

To determine the long-term immunity effect in vivo, engineered LLC cells were first subcutaneously implanted in the flank of immunocompetent C57BL/6 mice, and parental LLC-FmC cells were implanted orthotopically into their lungs 7 days later (Fig. 5C). BLI revealed aggressive tumor growth in the lungs of all mice from phosphate-buffered saline (PBS) and LLC-TC groups on day 7 after tumor implantation (Fig. 5D). All mice from the LLC-TC group were euthanized on day 10 after implantation in the lung because of the size of flank tumors (Fig. 5E). Despite no flank tumors, the median survival for mice from the PBS group was day 18 after implantation due to aggressive tumor growth in the

lung (Fig. 5E). In contrast, none of the mice from the LLC-ThTC group had tumor growth in the flank or the lung (Fig. 5D), and they survived for more than 30 days after implantation (Fig. 5E). This indicated that LLC-ThTCs induced antitumor immune responses to prevent tumor growth of LLC-FmC in the lung. Similar findings were also observed in the investigations of B16-ThTCs (fig. S8, C and D).

Given that brain metastasis is common for lung carcinoma, we rechallenged surviving mice from the LLC-ThTC group and the naïve C57BL/6 mice, as a control, with intracranial implantation of LLC-FmC cells (Fig. 5C). Seventy-five percent of the mice from the LLC-ThTC group survived rechallenge in the brain, whereas aggressive tumor growth was observed in all mice from the control group (Fig. 5F). This finding suggests that LLC-ThTCs induce long-term systemic immunological memory that can prevent distant metastasis of lung carcinoma.

In a resection model for LLC (Fig. 5G), tumors recurred (Fig. 5H), and the animals had to be euthanized on day 12 after treatment for the sECM-only group (Fig. 5I). Although a low Fluc signal was observed for mice in the LLC-TC group after treatment (Fig. 5H), large tumors likely arising from LLC-TCs meant that the mice had to be euthanized on day 12 after treatment (Fig. 5I). Conversely, residual tumor cells in the resection cavity were completely eradicated in all mice from the LLC-ThTC group on day 6 after resection (Fig. 5H), and these mice survived long term (Fig. 5I).

To determine whether these therapeutic cells can induce long-term immunity, we rechallenged the surviving mice in the right flank (Fig. 5G). No tumor growth was observed in the LLC-ThTC group, and mice survived long term (Fig. 5J). Thirty days later, we further rechallenged these surviving mice again in the brain (Fig. 5G). Although aggressive tumor growth was observed in the brains of naïve mice, no tumor growth was observed in the LLC-ThTC group, and mice survived long term (Fig. 5K). Consistent with GBM ThTCs, these findings suggest that LLC-ThTCs might also have a dual function of effectively killing residual tumor cells and inducing adaptive immunity that can prevent distant metastasis.

Implementation of double suicide system and generation of human ThTCs

To ensure the safety of using living tumor cells as a therapeutic approach, we further implemented an additional suicide system, a RapaCasp9-based safety switch (58) in the tumor cells. The sGBM cells were engineered to express both HSV-TK and RapaCasp9 as well as Fluc-mCherry, hereinafter referred to as "sGBM-RapaTK-FmC," using lentiviral transduction. Cell viability assay demonstrated that GCV (Fig. 6A) and rapamycin (Fig. 6B) potently suppressed cell viability of sGBM-RapaTK-FmC after 24 hours of treatment. An in vivo experiment (Fig. 6C) revealed complete tumor clearance in mice implanted with sGBM-RapaTK-FmC after 5 days of combined Rapa/GCV treatment administered 7 days after tumor inoculation, whereas tumors continued to grow in mice with sGBM-FmC with treatment and in mice with sGBM-RapaTK-FmC without treatment (Fig. 6D). This confirmed the effectiveness of our double suicide system in these tumor cells. In addition, no significant ($P > 0.05$) weight loss was observed throughout the treatment (table S9), and these mice survived for 30 days until the termination of the experiment, implying that the Rapa/GCV treatment was well tolerated.

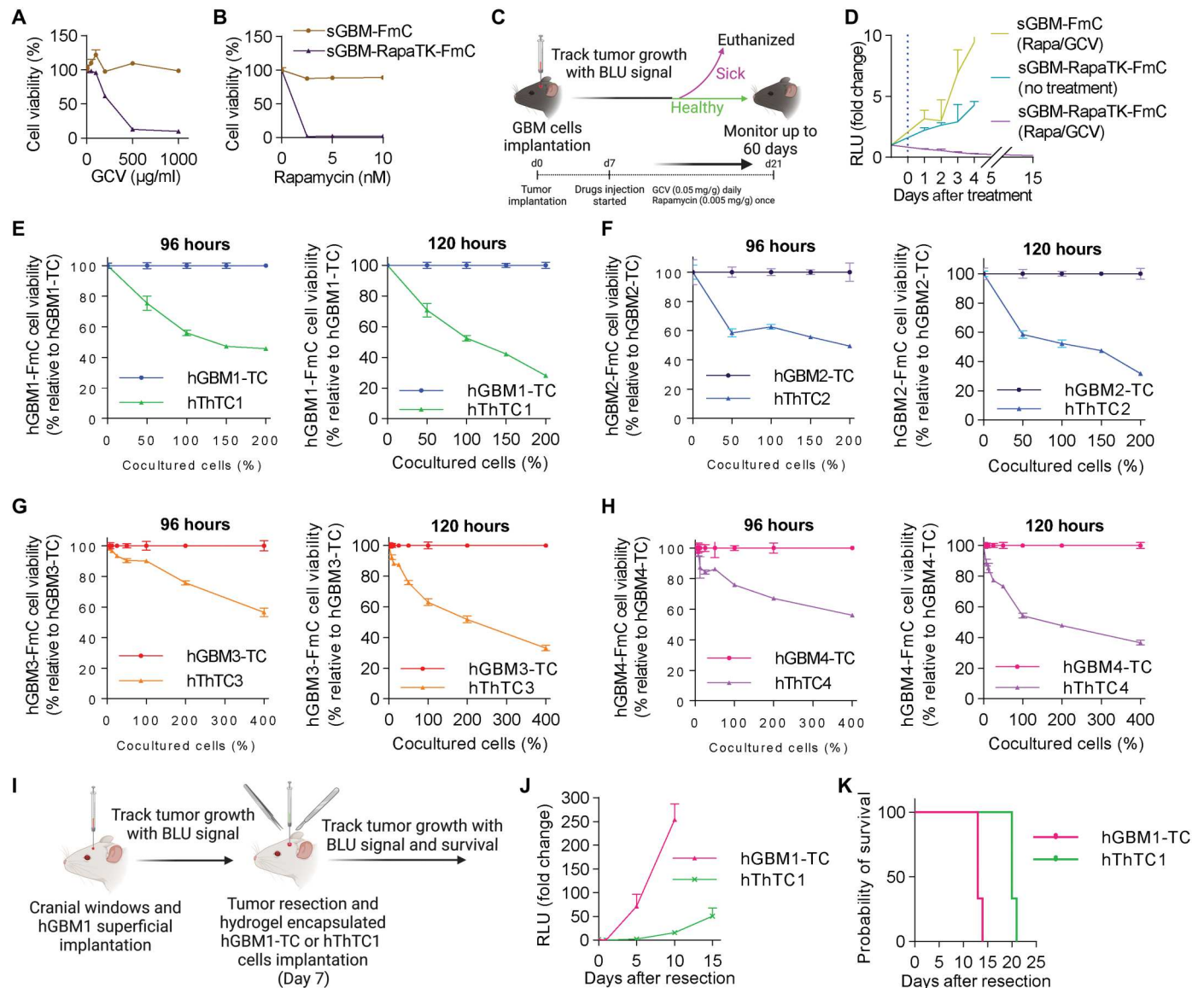


Fig. 6. Implementation of double suicide system in tumor cells and generation of human ThTCs. (A) Cell viability of sGBM-RapaTK-FmC treated with increasing concentrations of GCV. (B) Cell viability assay of sGBM-RapaTK-FmC treated with increasing concentrations of rapamycin. (C) Schematic of experimental timeline to investigate the efficacy of a double suicide system. (D) Fluc signal of C57BL/6 mice implanted with sGBM-FmC cells ($n = 3$) or sGBM-RapaTK-FmC cells, with ($n = 3$) or without ($n = 3$) rapamycin and GCV treatment. (E) Coculture of hGBM1-FmC cells (U87) and engineered hGBM1-TCs (hIFNAR1KO) or hThTC1 (hIFN-β/GM-CSF-expressing) cells for 96 hours (left) and 120 hours (right). (F) Coculture of hGBM2-FmC cells (LN229) and engineered hGBM2-TCs (hIFNAR1KO) or hThTC2 (hIFN-β/GM-CSF-expressing) cells for 96 hours (left) and 120 hours (right). (G) Coculture of hGBM3-FmC cells (GBM23) and engineered hGBM3-TCs (hIFNAR1KO) or hThTC3 (hIFN-β/GM-CSF-expressing) cells for 96 hours (left) and 120 hours (right). (H) Coculture of hGBM4-FmC cells (GBM4) and engineered hGBM4-TCs (hIFNAR1KO) or hThTC4 (hIFN-β/GM-CSF-expressing) cells for 96 hours (left) and 120 hours (right). (I) Schematic of experimental timeline for the GBM resection BLT mouse model. (J) Fluc signal in the hGBM1-bearing BLT mice after resection and treatment with either hGBM1-TC ($n = 3$) or hThTC1 ($n = 3$). (K) Kaplan-Meier showing the survival probability of the BLT mice after resection and treatment. Log-rank (Mantel-Cox) test. $P < 0.05$.

Therapeutic effects of human ThTCs in vitro and in vivo

To translate our findings into the patient settings, we CRISPR-knocked out human *IFNAR1* in two established human GBM cell lines, hGBM1 and hGBM2, and patient-derived GBM cells, hGBM3 and hGBM4, referred to as hGBM-TC, and transduced them with the lentiviral vector encoding human IFN-β and GM-CSF to generate hThTCs. IFNAR1 expression in hGBM3 and hGBM4 was confirmed using flow cytometry (fig. S9, A and B). Dose-dependent

cytotoxicity was observed when these engineered hThTCs were cocultured with their respective parental GBM lines at varying ratios (Fig. 6, E to H), indicating their ability to kill tumor cells. Cytotoxicity was increased for all human ThTCs after extending the coculture duration from 96 to 120 hours (Fig. 6, E to H).

To further demonstrate the therapeutic efficacy of ThTCs in a setting that recapitulates the human immune microenvironment in vivo, we used the BLT (bone marrow, liver, and thymus)

humanized mice to create a human GBM resection model. Specifically, humanized mice bearing resected human GBMs (hGBM1) were treated with sECM-encapsulated hGBM1-TC or hThTC1 (Fig. 6I). The treatment with hThTC1 suppressed hGBM1 tumor growth and improved the survival of tumor-bearing mice after treatment compared with hGBM1-TC control (Fig. 6, J and K). Together, these data demonstrate the safety, applicability, and efficacy of our tumor cell-based therapeutic strategy for various tumor types in both immunocompetent and humanized mouse models, thereby establishing a road map toward clinical translation.

DISCUSSION

This study demonstrates the therapeutic potential of using engineered living tumor cells to therapeutically treat tumors and to convert the immunosuppressive TME into an immunostimulatory TME. Here, we show that ThTCs induce programmed cell death not only by down-regulating cell cycle signaling but also by down-regulating CAF-expressed PDGFRB. ThTCs also promote durable antitumor immune responses by modulating immune cell trafficking and signaling.

Although no model exactly recapitulates human GBM, each has unique features that should be considered when designing preclinical experiments. Given that this study is a preclinical investigation into the use of immunotherapies where a fully functional immune system is required, syngeneic mouse models are preferred over other model types. Syngeneic transplantation models also allow orthotopic implantation superficially and subsequent resection to mimic the clinical scenario of surgical debulking. We chose sGBM (CT2A) based on our previous detailed characterization of the immune microenvironment of different syngeneic models, demonstrating sGBM to be one of the most aggressive and sGBM syngeneic models (39). Although genetically engineered mouse models such as replication-competent avian sarcoma leukosis virus long repeat with a splice acceptor (RCAS) system (59, 60) provide immunocompetent GBM models and their defined genetic alterations are suitable for studying genetic phenotype relationships, the immune microenvironment in these models is less defined.

IFN- β has immune-stimulatory effects on various immune cells, including tumor-specific T lymphocytes, B lymphocytes, and DCs (61). This cytokine is also a determinant of the efficacy of antitumor immunity (62). In this study, we genetically engineered tumor cells to release a secretable variant of IFN- β (63) for on-site delivery of IFN- β to the TME. There are several advantages of using tumor cells for local delivery of IFN- β to the TME over other types of cellular carriers such as mesenchymal stem cells (63) or myeloid cells (64). First, tumor cells are highly proliferative, which provides an easy process of expansion and genetic engineering *ex vivo* as well as a prolonged secretion of IFN- β at the tumor site when used for treatment. Second, tumor cells, especially patient-specific autologous tumor cells, are a source of neoantigens, which potentially facilitate antigen-specific T cell immunity against the tumor. However, almost all tumor cells express *IFNARI2* (Fig. 1C and fig. S1I) and might be sensitive to IFN- β themselves. Therefore, IFN- β -secreting tumor cells are subject to the autocrine toxicity as seen in previous studies (25, 27, 28). To our knowledge, this is the first study to demonstrate the creation of tumor cells that stably

secrete IFN- β and with prior receptor knockout using CRISPR technology.

The integration of GM-CSF together with IFN- β secretion by the ThTCs further improved their antitumor effects (Fig. 2C) and induced long-term immunological memory (Fig. 2E), suggesting additive antitumor effects. The depletion of either CD4⁺ or CD8⁺ T cells did not abolish the tumor growth inhibitory effects elicited by ThTCs, implying that CD4⁺ and CD8⁺ T cells can function independently in eliminating tumor cells. It is well known that CD8⁺ cytotoxic T lymphocytes have a role in tumor killing in immunotherapy, and there is much less emphasis on the role and contribution of CD4⁺ T cells. According to previous studies, CD4⁺ T cells are able to differentiate into T helper type 1 cytotoxic T cells *in vivo* and induce tumor regression independent of CD8⁺ T cells or NK cells (65, 66). Our data showed that the TMEs of mice treated with ThTCs had elevated expression of a cytotoxic CD4⁺ T cell signature (fig. S6G) as well as common surface biomarkers and upstream inducers for cytotoxic CD4⁺ T cell in comparison with sECM-only and GFP-TC groups (fig. S6H). These data further imply that ThTCs are able to activate the cytotoxic function of CD4⁺ T cells. On the other hand, mice with CD4⁺ T cell depletion failed to develop a durable immune response that could counter rechallenge with wild-type tumor cells (Fig. 2M). This implies a role of functional memory CD4⁺ T cells in maintaining immune surveillance for preventing tumor growth and progression.

In our preclinical GBM resection model, the introduction of ThTCs eradicated the residual tumor by activating apoptosis (Fig. 3, E and F) and down-regulating PDGFRB at both mRNA (Fig. 4E and fig. S6E) and protein (Fig. 4, G and H) levels. *PDGFRB* is a well-known GBM oncogene that promotes glioma stem cell growth, survival, and invasion (67). The expression of *STAT1*, a downstream IFN-stimulated gene, has a negative correlation with *PDGFRB* expression in fibroblasts (68), which suggests an indirect regulation of IFN- β /GM-CSF expression to prevent tumor growth and progression.

Considering the time needed to engineer autologous cell lines, it would be challenging to use the ThTC strategy for primary GBM treatment. Although this might become possible with the advances in genetic engineering, in current settings, the treatment with ThTCs should be aimed at the therapy of recurrent or metastatic disease. Therefore, our studies also demonstrate the feasibility and therapeutic efficacy of this CRISPR-edited ThTC-based therapeutic strategy in clinically relevant mouse models of recurrent (fig. S7) and metastatic cancers (Fig. 5 and fig. S8), highlighting the potential application to multiple solid tumor malignancies and stages of tumor progression.

Given the beneficial immune responses elicited by our ThTCs at the tumor site and to ensure a prolonged supply of therapeutic agents, we used ThTCs as a living and active form in our preclinical models without prior inactivation or irradiation as seen in other studies (1–3). However, one of the main concerns of using cancer cells as a therapeutic is their tumorigenic potential. We integrated a prodrug-activatable suicide system to address this concern. Although the implantation of our ThTCs did not form tumors in mice with intact immune systems (Fig. 2B), we demonstrate that tumors developed in immunodeficient mice and these therapeutic cancer cells expressing HSV-TK can be safely eliminated with GCV treatment *in vivo*, and no tumor relapse was observed (Fig. 2, F and G). This is consistent with the findings in clinical studies where a

robust safety profile of HSV-TK systems was observed when used in proliferating cells in patients (69, 70). In addition, we further introduced an additional RapaCasp9-based suicide gene (58) in the tumor cells to provide another layer of security toward translating these therapeutic cancer cells into the clinic (Fig. 6, A to D).

The therapeutic effects *in vivo* are dependent not only on direct cytotoxicity to the tumor but also on the antitumor immune responses elicited by ThTCs. In addition to inhibiting the growth and progression of residual tumor after resection, the direct cytotoxicity of ThTCs also contributes to the antigen spread after tumor cell death. Tumor antigens can be presented and cross-presented by DCs, thereby activating tumor-specific immune responses with the aid of IFN- β and GM-CSF secreted by ThTCs to promote tumor eradication and immunity. This is corroborated by our GBM resection experiments using BLT humanized mice, where human ThTCs are able to improve the survival of mice bearing human GBM (Fig. 6, I to K). Although optimization of the treatment regimen is still required for the BLT humanized mouse model, our data demonstrate the feasibility and efficiency of our proposed immunotherapeutic approach for GBM and advances clinical translation.

There are several limitations to this study. As discussed earlier, the syngeneic transplantation model enabled us to mimic the clinical scenario of surgical debulking in this study; however, we recognize that tumor engraftment is not how GBM arises and therefore cannot completely recapitulate the TME. A potential follow-up study could be evaluating the therapeutic potential of ThTCs using spontaneous GBM mouse models, such as an RCAS system after extensive immunophenotyping on the model. In this study, we observed a durable systemic immunological memory induced by ThTCs in the mouse models. This immunological effect is likely linked to the recognition of neoantigens expressed by ThTCs and derived from tumor cell death upon treatment. However, further investigations are required to understand the mechanisms of how ThTC-based therapy activates tumor antigen presentation and tumor-specific T cell immunity.

Together, our study establishes a bifunctional cancer cell-based therapeutic strategy that can directly target tumor cells and indirectly induce immune-mediated cell death and durable immunity to prevent tumor recurrence and progression. Our investigations suggest that the introduction of IFN- β /GM-CSF-secreting ThTCs into the resection cavity can result in transcriptional and cellular reprogramming, converting the immunoinhibitory TME into an immunostimulatory TME. Exhibiting robustness and wide applicability, this therapeutic strategy using ThTCs has the potential to affect patients by preventing tumor progression, recurrence, and metastasis. We envision that this bifunctional therapeutic cancer cell could offer a personalized cellular therapy and ultimately improve clinical outcomes for patients with cancer.

MATERIALS AND METHODS

Study design

The objective of this study was to develop an efficient therapeutic strategy that can simultaneously induce a direct killing of tumor cells and elicit antitumor immune responses to counter the tumor aggressiveness and the immunosuppressive microenvironment. We hypothesized that genetic engineering of cancer cells would allow us to use and repurpose their self-homing and neoantigen-rich

features for cancer treatment. All experiments performed in this study had at least three replicates to demonstrate biological reproducibility and to ensure adequate statistical power for comparisons. All animals were randomly allocated to the control and treatment groups with equivalent tumor size. The study was not blinded, and no statistical methods were used to predetermine the sample size. Details for *in vivo* experiments, number of cells used, duration, and statistical tests are described below, in the Supplementary Materials, and in the figure legends.

Intracranial deep implantation

C57BL/6, SCID, or nude mice were anesthetized and immobilized on a stereotactic frame. Tumor cells (2×10^5) in 3 μ l of PBS were implanted 2.2 mm deep, 2.5 mm lateral from bregma, and 2.5 mm ventral from dura in the left hemisphere for the first implantation and in the right hemisphere for the rechallenge.

Intracranial resection model

C57BL/6, NOD SCID, or BLT humanized mice were used for this procedure. Cranial windows were created by removing ~1 mm diameter of the skull 2 mm lateral from the bregma and 2 mm ventral from dura in the right hemisphere of anesthetized mice. Tumor cells (2×10^5) in 3 μ l of PBS were implanted 0.7 mm deep in the cranial window. Tumor growth was checked by BLI every 3 days. Fluorescence-guided resection was performed. A total of 1×10^6 cells were encapsulated with sECM hydrogel (#HYSC020-1KT, Sigma-Aldrich) and administered onto the resection cavity as treatment on day 10 after tumor implantation. Tumors were analyzed before and after treatment by BLI.

TMZ-resistant rGBM line establishment

C57BL/6 mice were intracranially implanted with sGBM-FmC and administered with TMZ intraperitoneally daily for 5 days starting from day 6 after implantation (fig. S7A). When these TMZ-treated mice reached the clinical end point, the tumor tissues were harvested and dissociated for cell culture as rGBM-FmC.

Subcutaneous tumor implantation

C57BL/6 mice were anesthetized, and 5×10^5 tumor cells in 100 μ l of PBS with 50% Matrigel (#356234, Corning) were implanted under the skin into the subcutaneous tissue on the left or right flanks of the mice.

Subcutaneous tumor resection

C57BL/6 mice were used in this procedure. Subcutaneous tumors were allowed to grow to 1 cm³ until the resection. A total of 1×10^6 cells were encapsulated with sECM hydrogel and administered onto the resection cavity as treatment.

Lung tumor implantation

C57BL/6 mice were anesthetized, and 1×10^5 tumor cells in 20 μ l of PBS with 50% Matrigel were implanted into the intercostal space between ribs 5 and 6 of the right lung.

Mouse brain tissue harvest

C57BL/6, SCID, NOD/SCID, and BLT humanized mice were perfused with 10 ml of PBS by cardiac puncture. For immunofluorescence analyses, mice were further perfused with 10 ml of 10% buffered formalin (Thermo Fisher Scientific) for fixation, and

brains were harvested. For immune profiling, tumor tissues were harvested and processed for flow cytometry analysis. For RNA-seq, tumor tissues were harvested and processed for RNA extraction.

Lentiviral transductions and engineering of stable cell lines

Lentiviral packaging was performed by transfection of 293T cells as previously described (71), and cells were transduced with lentiviral vectors at a multiplicity of infection (MOI) of 2 in medium containing protamine sulfate (2 µg/ml). For BLI, cancer cells were transduced with LV-Pico2-Fluc-mCherry and selected by fluorescence-activated cell sorting (FACS) using a BD FACSAria Fusion cell sorter or puromycin selection (1 µg/ml) in culture. GFP or mCherry expression was confirmed by fluorescence microscopy.

For mouse *Ifnar1* knockout, top and bottom strands of single-guide RNA (sgRNA) oligos were aligned as previously described (72), followed by cloning strategy as previously described (19) into PX459 plasmid (Addgene, plasmid 48139) using restriction enzyme Bbs I. U6-sgRNA regions of sequencing-confirmed PX459-sgRNA clones were PCR-amplified with the following primers containing flanking gateway-attB1 and gateway-attB2 sequences, respectively: attB1-forward, 5'-GGGGACAAGTTTGTCAAAAAAGCAGGGTCCGAGGGCC TATTTCCCATGATT-3' and attB2-reverse, 5'-GGGGACCACTTTGTACAAGAAAGCTGGGTCTCTAGAGCCATTTGTC TGCAG-3'. To prepare gateway entry clones, the amplified PCR products were gel-extracted, purified, and cloned into pDONR201 vector (Invitrogen) using the gateway BP reaction. The lentiviral cDNA/short hairpin-mediated RNA gateway vectors pLKO.DEST.egfp (Addgene, plasmid 32684) or pLKO.DEST.hygro (Addgene, plasmid 32685) served as destination vectors after gateway LR reaction. All destination sgRNA expression vectors were sequenced to confirm correct U6-sgRNA inserts before proceeding with third-generation lentiviral packaging. For targeting of mouse *Ifnar1*, either CACTGCCCATTTGACTCTCCGTGG or TTCGTGTCAGAGCAGAGGAAGGG was used.

To establish knockout mouse lines, we transduced cells with lentiviral Cas9 expression vectors coding for either tetracycline-inducible or constitutively expressed Cas9 protein as previously described (73, 74). Confirmed Cas9 lines were engineered with lentiviral sgRNA expression vector pLKO.DEST.hygro containing the sgRNA target sequences described above, followed by selection with hygromycin (200 to 500 µg/ml). To screen for knockout efficacy, we analyzed whole-cell lysates of mixed populations for sensitivity to respective ligands in comparison with non-engineered controls. Candidate populations were then clonally selected, followed by screening of individual clones for knockout status with Western blotting of cell lysates. To analyze knockout clones for targeted indel formation, we isolated genomic DNA from clonal cell populations as previously described (75), and the following primers were used for sequencing of target regions: *Ifnar1* exon 2, CTTTCTGTACCGTACTGGTCATT (forward) and TCTCAGCTCAGTCTCCACGG (reverse) and *Ifnar1* exon 3, AACACGTTTTAAAAGCCCATGTAT (forward) and GGACCTGCTAAAA GGCTCTTGA (reverse). To establish IFN-β-expressing cell lines, cells were transduced with lentiviral pRRL.ppt.EFS.GFP vector with mIFN-β (63) and HSV-TK (19) genes and selected by FACS using a BD FACSAria Fusion cell sorter. To establish GM-CSF-expressing cell lines, cells were transduced with lentiviral pico2-

mCherry vector with GM-CSF gene (UniProtKB, P01587) and selected by puromycin (2 µg/ml) treatment.

For human *IFNAR1* knockout, top and bottom strands of sgRNA oligos were aligned as previously described (73), followed by cloning strategy into lentiCRISPRv2GFP plasmid (Addgene, plasmid 82416) using restriction enzyme Bsm BI. All destination sgRNA expression vectors were sequenced to confirm correct U6-sgRNA inserts before proceeding with third-generation lentiviral packaging. For targeting of human *IFNAR1*, TAACCATGTGACTACTAACGTGG was used. To establish cell lines expressing human IFN-β, GM-CSF, and HSV-TK, cells were transduced with lentiviral pRRL.ppt.EFS.GFP vector with the secretable human IFN-β (63), GM-CSF (UniProtKB, P04141), and HSV-TK (19) genes and selected by FACS using a BD FACSAria Fusion cell sorter.

Statistical analysis

Data were expressed as means ± SD for in vitro studies and ±SEM for in vivo studies and analyzed by Student's *t* test or analysis of variance (ANOVA) with Holm-Šidák test for multiple comparisons correction. Survival times of mouse groups were analyzed and compared using log-rank (Mantel-Cox) test and Bonferroni correction. GraphPad Prism 9 software was used for all statistical analysis and also to generate Kaplan-Meier survival plots. Differences were considered significant at **P* < 0.05, ***P* < 0.01, ****P* < 0.001, and *****P* < 0.0001.

Supplementary Materials

This PDF file includes:

Materials and Methods

Figs. S1 to S9

References (76–78)

Other Supplementary Material for this manuscript includes the following:

Data file S1

Tables S1 to S9

MDAR Reproducibility Checklist

[View/request a protocol for this paper from Bio-protocol.](#)

REFERENCES AND NOTES

1. M. Moehler, M. Zeidler, J. Schede, J. Rommelaere, P. R. Galle, J. J. Cornelis, M. Heike, Oncolytic parvovirus H1 induces release of heat-shock protein HSP72 in susceptible human tumor cells but may not affect primary immune cells. *Cancer Gene Ther.* **10**, 477–480 (2003).
2. G. Dranoff, E. Jaffee, A. Lazenby, P. Golumbek, H. Levitsky, K. Brose, V. Jackson, H. Hamada, D. Pardoll, R. C. Mulligan, Vaccination with irradiated tumor cells engineered to secrete murine granulocyte-macrophage colony-stimulating factor stimulates potent, specific, and long-lasting anti-tumor immunity. *Proc. Natl. Acad. Sci. U.S.A.* **90**, 3539–3543 (1993).
3. T. F. Greten, E. M. Jaffee, Cancer vaccines. *J. Clin. Oncol.* **17**, 1047–1060 (1999).
4. R. O. Dillman, A. N. Cornforth, G. I. Nistor, E. F. McClay, T. T. Amatruda, C. Depriest, Randomized phase II trial of autologous dendritic cell vaccines versus autologous tumor cell vaccines in metastatic melanoma: 5-year follow up and additional analyses. *J. Immunother. Cancer* **6**, 19 (2018).
5. W. T. Curry Jr., R. Gorrepati, M. Piesche, T. Sasada, P. Agarwalla, P. S. Jones, E. R. Gerstner, A. J. Golby, T. T. Batchelor, P. Y. Wen, M. C. Mihm, G. Dranoff, Vaccination with irradiated autologous tumor cells mixed with irradiated GM-K562 cells stimulates antitumor immunity and T lymphocyte activation in patients with recurrent malignant glioma. *Clin. Cancer Res.* **22**, 2885–2896 (2016).
6. V. Schirmmacher, P. Fournier, P. Schlag, Autologous tumor cell vaccines for post-operative active-specific immunotherapy of colorectal carcinoma: Long-term patient survival and mechanism of function. *Expert Rev. Vaccines* **13**, 117–130 (2014).

7. R. Soiffer, T. Lynch, M. Mihm, K. Jung, C. Rhuda, J. C. Schmollinger, F. S. Hodi, L. Lieber, P. Lam, S. Mentzer, S. Singer, K. K. Tanabe, A. B. Cosimi, R. Duda, A. Sober, A. Bhan, J. Daley, D. Neuberg, G. Parry, J. Rokovich, L. Richards, J. Drayer, A. Berns, S. Clift, L. K. Cohen, R. C. Mulligan, G. Dranoff, Vaccination with irradiated autologous melanoma cells engineered to secrete human granulocyte-macrophage colony-stimulating factor generates potent antitumor immunity in patients with metastatic melanoma. *Proc. Natl. Acad. Sci. U.S.A.* **95**, 13141–13146 (1998).
8. M. S. Sasso, N. Mitrousis, Y. Wang, P. S. Briquez, S. Hauert, J. Ishihara, J. A. Hubbell, M. A. Swartz, Lymphangiogenesis-inducing vaccines elicit potent and long-lasting T cell immunity against melanomas. *Sci. Adv.* **7**, eabe4362 (2021).
9. R. O. Dillman, S. K. Nayak, N. M. Barth, L. S. Schwartzberg, L. E. Spitzer, C. Church, A. A. O'Connor, L. D. Beutel, Clinical experience with autologous tumor cell lines for patient-specific vaccine therapy in metastatic melanoma. *Cancer Biother. Radiopharm.* **13**, 165–176 (1998).
10. R. O. Dillman, C. DeLeon, L. D. Beutel, N. M. Barth, L. S. Schwartzberg, L. E. Spitzer, D. H. Garfield, A. A. O'Connor, S. K. Nayak, Short-term autologous tumor cell lines for the active specific immunotherapy of patients with metastatic melanoma. *Crit. Rev. Oncol. Hematol.* **39**, 115–123 (2001).
11. R. O. Dillman, N. M. Barth, L. A. VanderMolen, D. H. Garfield, C. De Leon, A. A. O'Connor, K. Mahdavi, S. K. Nayak, Treatment of kidney cancer with autologous tumor cell vaccines of short-term cell lines derived from renal cell carcinoma. *Cancer Biother. Radiopharm.* **16**, 47–54 (2001).
12. R. O. Dillman, L. D. Beutel, C. De Leon, S. K. Nayak, Short-term tumor cell lines from breast cancer for use as autologous tumor cell vaccines in the treatment of breast cancer. *Cancer Biother. Radiopharm.* **16**, 205–211 (2001).
13. R. O. Dillman, S. K. Nayak, J. V. Brown, K. Mahdavi, L. D. Beutel, The feasibility of using short-term cultures of ovarian cancer cells for use as autologous tumor cell vaccines as adjuvant treatment of advanced ovarian cancer. *Cancer Biother. Radiopharm.* **14**, 443–449 (1999).
14. D. T. Le, V. J. Picozzi, A. H. Ko, Z. A. Wainberg, H. Kindler, A. Wang-Gillam, P. Oberstein, M. A. Morse, H. J. Zeh III, C. Weekes, T. Reid, E. Borazanci, T. Croceni, N. K. LoConte, B. Musher, D. Laheru, A. Murphy, C. Whiting, N. Nair, A. Enstrom, S. Ferber, D. G. Brockstedt, E. M. Jaffee, Results from a phase IIb, randomized, multicenter study of GVAX pancreas and CRS-207 compared with chemotherapy in adults with previously treated metastatic pancreatic adenocarcinoma (ECLIPSE Study). *Clin. Cancer Res.* **25**, 5493–5502 (2019).
15. A. A. Wu, K. M. Bever, W. J. Ho, E. J. Fertig, N. Niu, L. Zheng, R. M. Parkinson, J. N. Durham, B. Onners, A. K. Ferguson, C. Wilt, A. H. Ko, A. Wang-Gillam, D. A. Laheru, R. A. Anders, E. D. Thompson, E. A. Sugar, E. A. Jaffee, D. T. Le, A phase II study of allogeneic GM-CSF-transfected pancreatic tumor vaccine (GVAX) with ipilimumab as maintenance treatment for metastatic pancreatic cancer. *Clin. Cancer Res.* **26**, 5129–5139 (2020).
16. E. Dondossola, A. S. Dobroff, S. Marchio, M. Cardo-Vila, H. Hosoya, S. K. Libutti, A. Corti, R. L. Sidman, W. Arap, R. Pasqualini, Self-targeting of TNF-releasing cancer cells in pre-clinical models of primary and metastatic tumors. *Proc. Natl. Acad. Sci. U.S.A.* **113**, 2223–2228 (2016).
17. M. Y. Kim, T. Oskarsson, S. Acharyya, D. X. Nguyen, X. H. Zhang, L. Norton, J. Massague, Tumor self-seeding by circulating cancer cells. *Cell* **139**, 1315–1326 (2009).
18. L. Norton, J. Massague, Is cancer a disease of self-seeding? *Nat. Med.* **12**, 875–878 (2006).
19. C. Reinshagen, D. Bhere, S. H. Choi, S. Hutten, I. Nesterenko, H. Wakimoto, E. Le Roux, A. Rizvi, W. Du, C. Minicucci, K. Shah, CRISPR-enhanced engineering of therapy-sensitive cancer cells for self-targeting of primary and metastatic tumors. *Sci. Transl. Med.* **10**, eaao3240 (2018).
20. J. Y. Zhu, D. W. Zheng, M. K. Zhang, W. Y. Yu, W. X. Qiu, J. J. Hu, J. Feng, X. Z. Zhang, Preferential cancer cell self-recognition and tumor self-targeting by coating nanoparticles with homotypic cancer cell membranes. *Nano Lett.* **16**, 5895–5901 (2016).
21. T. G. Johns, I. R. Mackay, K. A. Callister, P. J. Hertzog, R. J. Devenish, A. W. Linnane, Anti-proliferative potencies of interferons on melanoma cell lines and xenografts: Higher efficacy of interferon beta. *J. Natl. Cancer Inst.* **84**, 1185–1190 (1992).
22. M. G. Rosenblum, W. K. Yung, P. J. Kelleher, F. Ruzicka, P. A. Steck, E. C. Borden, Growth inhibitory effects of interferon- β but not interferon- α on human glioma cells: Correlation of receptor binding, 2',5'-oligoadenylate synthetase and protein kinase activity. *J. Interferon Res.* **10**, 141–151 (1990).
23. L. Zitvogel, L. Galluzzi, O. Kepp, M. J. Smyth, G. Kroemer, Type I interferons in anticancer immunity. *Nat. Rev. Immunol.* **15**, 405–414 (2015).
24. K. Pokrovskaja, T. Panaretakis, D. Grandier, Alternative signaling pathways regulating type I interferon-induced apoptosis. *J. Interferon Cytokine Res.* **25**, 799–810 (2005).
25. Z. Dong, G. Greene, C. Pettaway, C. P. Dinney, I. Eue, W. Lu, C. D. Bucana, M. D. Balbay, D. Bielenberg, I. J. Fidler, Suppression of angiogenesis, tumorigenicity, and metastasis by human prostate cancer cells engineered to produce interferon- β . *Cancer Res.* **59**, 872–879 (1999).
26. J. Jablonska, S. Leschner, K. Westphal, S. Lienenklaus, S. Weiss, Neutrophils responsive to endogenous IFN- β regulate tumor angiogenesis and growth in a mouse tumor model. *J. Clin. Invest.* **120**, 1151–1164 (2010).
27. A. A. Lykhova, Y. I. Kudryavets, L. I. Strokovska, N. A. Bezdenezhnykh, N. I. Semesiuik, I. N. Adamenko, O. V. Anoprienko, A. L. Vorontsova, Suppression of proliferation, tumorigenicity and metastasis of lung cancer cells after their transduction by interferon-beta gene in baculovirus vector. *Cytokine* **71**, 318–326 (2015).
28. X. Q. Qin, N. Tao, A. Dergay, P. Moy, S. Fawell, A. Davis, J. M. Wilson, J. Barsoum, Interferon-beta gene therapy inhibits tumor formation and causes regression of established tumors in immune-deficient mice. *Proc. Natl. Acad. Sci. U.S.A.* **95**, 14411–14416 (1998).
29. J. A. Hamilton, A. Achuthan, Colony stimulating factors and myeloid cell biology in health and disease. *Trends Immunol.* **34**, 81–89 (2013).
30. L. Min, S. A. Mohammad Isa, W. Shuai, C. B. Piang, F. W. Nih, M. Kotaka, C. Ruedl, Cutting edge: Granulocyte-macrophage colony-stimulating factor is the major CD8⁺ T cell-derived licensing factor for dendritic cell activation. *J. Immunol.* **184**, 4625–4629 (2010).
31. Y. Chu, L. X. Wang, G. Yang, H. J. Ross, W. J. Urba, R. Prell, K. Jooss, S. Xiong, H. M. Hu, Efficacy of GM-CSF-producing tumor vaccine after docetaxel chemotherapy in mice bearing established Lewis lung carcinoma. *J. Immunother.* **29**, 367–380 (2006).
32. S. Gillesen, Y. N. Naumov, E. E. Nieuwenhuis, M. A. Exley, F. S. Lee, N. Mach, A. D. Luster, R. S. Blumberg, M. Taniguchi, S. P. Balk, J. L. Strominger, G. Dranoff, S. B. Wilson, CD1d-restricted T cells regulate dendritic cell function and antitumor immunity in a granulocyte-macrophage colony-stimulating factor-dependent fashion. *Proc. Natl. Acad. Sci. U.S.A.* **100**, 8874–8879 (2003).
33. N. Mach, S. Gillesen, S. B. Wilson, C. Sheehan, M. Mihm, G. Dranoff, Differences in dendritic cells stimulated in vivo by tumors engineered to secrete granulocyte-macrophage colony-stimulating factor or Flt3-ligand. *Cancer Res.* **60**, 3239–3246 (2000).
34. Z. Qin, G. Noffz, M. Mohaupt, T. Blankenstein, Interleukin-10 prevents dendritic cell accumulation and vaccination with granulocyte-macrophage colony-stimulating factor gene-modified tumor cells. *J. Immunol.* **159**, 770–776 (1997).
35. Z. Zhao, K. N. Zhang, Q. Wang, G. Li, F. Zeng, Y. Zhang, F. Wu, R. Chai, Z. Wang, C. Zhang, W. Zhang, Z. Bao, T. Jiang, Chinese Glioma Genome Atlas (CGGA): A comprehensive resource with functional genomic data from chinese glioma patients. *Genom. Proteom. Bioinform.* **19**, 1–12 (2021).
36. V. Thorsson, D. L. Gibbs, S. D. Brown, D. Wolf, D. S. Bortone, T. H. O. Yang, E. Porta-Pardo, G. F. Gao, C. L. Plaisier, J. A. Eddy, E. Ziv, A. C. Culhane, E. O. Paull, I. K. A. Sivakumar, A. J. Gentles, R. Malhotra, F. Farshidfar, A. Colaprico, J. S. Parker, L. E. Mose, N. S. Vo, J. Liu, Y. Liu, J. Rader, V. Dhankani, S. M. Reynolds, R. Bowlby, A. Califano, A. D. Cherniack, D. Anastassiou, D. Bedognetti, Y. Mokrab, A. M. Newman, A. Rao, K. Chen, A. Krasnitz, H. Hu, T. M. Malta, H. Noshmeh, C. S. Pedamallu, S. Bullman, A. I. Ojesina, A. Lamb, W. Zhou, H. Shen, T. K. Choueiri, J. N. Weinstein, J. Guinney, J. Saltz, R. A. Holt, C. S. Rabkin; Cancer Genome Atlas Research Network, A. J. Lazar, J. S. Serody, E. G. Demicco, M. L. Disis, B. G. Vincent, I. Shmulevich, The immune landscape of cancer. *Immunity* **48**, 812–830.e814 (2018).
37. C. P. Dancy, J. Reidy, *Statistics without maths for psychology: Using SPSS for Windows*. (Pearson/Prentice Hall, Harlow, England, New York, ed. 4, 2007), pp. xxvi, p. 619.
38. A. P. Patel, I. Tirosh, J. J. Trombetta, A. K. Shalek, S. M. Gillespie, H. Wakimoto, D. P. Cahill, B. V. Nahed, W. T. Curry, R. L. Martuza, D. N. Louis, O. Rozenblatt-Rosen, M. L. Suva, A. Regev, B. E. Bernstein, Single-cell RNA-seq highlights intratumoral heterogeneity in primary glioblastoma. *Science* **344**, 1396–1401 (2014).
39. J. K. Khalsa, N. Cheng, J. Keegan, A. Chaudry, J. Driver, W. L. Bi, J. Lederer, K. Shah, Immune phenotyping of diverse syngeneic murine brain tumors identifies immunologically distinct types. *Nat. Commun.* **11**, 3912 (2020).
40. S. Kaczanowska, D. W. Beury, V. Gopalan, A. K. Tycko, H. Qin, M. E. Clements, J. Drake, C. Nwanze, M. Murgai, Z. Rae, W. Ju, K. A. Alexander, J. Kline, C. F. Contreras, K. M. Wessel, S. Patel, S. Hannehalli, M. C. Kelly, R. N. Kaplan, Genetically engineered myeloid cells rebalance the core immune suppression program in metastasis. *Cell* **184**, 2033–2052.e21 (2021).
41. A. D. Garg, L. Vandenberk, C. Koks, T. Verschuere, L. Boon, S. W. Van Gool, P. Agostinis, Dendritic cell vaccines based on immunogenic cell death elicit danger signals and T cell-driven rejection of high-grade glioma. *Sci. Transl. Med.* **8**, 328ra327 (2016).
42. L. M. Shelton, P. Mukherjee, L. C. Huysentruyt, I. Urits, J. A. Rosenberg, T. N. Seyfried, A novel pre-clinical in vivo mouse model for malignant brain tumor growth and invasion. *J. Neurooncol* **99**, 165–176 (2010).
43. B. Cohen, D. Novick, S. Barak, M. Rubinstein, Ligand-induced association of the type I interferon receptor components. *Mol. Cell. Biol.* **15**, 4208–4214 (1995).
44. P. Domanski, E. Fish, O. W. Nadeau, M. Witte, L. C. Platanias, H. Yan, J. Krolewski, P. Pitha, O. R. Colamonic, A region of the beta subunit of the interferon α receptor different from box 1 interacts with Jak1 and is sufficient to activate the Jak-Stat pathway and induce an antiviral state. *J. Biol. Chem.* **272**, 26388–26393 (1997).

45. R. P. Custer, G. C. Bosma, M. J. Bosma, Severe combined immunodeficiency (SCID) in the mouse. Pathology, reconstitution, neoplasms. *Am. J. Pathol.* **120**, 464–477 (1985).
46. L. R. Kelland, Of mice and men: Values and liabilities of the athymic nude mouse model in anticancer drug development. *Eur. J. Cancer* **40**, 827–836 (2004).
47. J. F. Hair, *Multivariate data analysis*. (Prentice Hall, Upper Saddle River, NJ, ed. 7th, 2010), pp. xxviii, 785 p.
48. S. I. Mosely, J. E. Prime, R. C. Sainson, J. O. Koopmann, D. Y. Wang, D. M. Greenawalt, M. J. Ahdesmaki, R. Leyland, S. Mullins, L. Pacelli, D. Marcus, J. Anderton, A. Watkins, J. Coates Ulrichsen, P. Brohawn, B. W. Higgs, M. McCourt, H. Jones, J. A. Harper, M. Morrow, V. Valge-Archer, R. Stewart, S. J. Dovedi, R. W. Wilkinson, Rational selection of syngeneic preclinical tumor models for immunotherapeutic drug discovery. *Cancer Immunol. Res.* **5**, 29–41 (2017).
49. A. Cachot, M. Bilous, Y. C. Liu, X. Li, M. Saillard, M. Cenerenti, G. A. Rockinger, T. Wyss, P. Guillaume, J. Schmidt, R. Genolet, G. Ercolano, M. P. Protti, W. Reith, K. Ioannidou, L. de Leval, J. A. Trapani, G. Coukos, A. Harari, D. E. Speiser, A. Mathis, D. Gfeller, H. Altug, P. Romero, C. Jandus, Tumor-specific cytolytic CD4 T cells mediate immunity against human cancer. *Sci. Adv.* **7**, eabe3348 (2021).
50. J. G. Burel, S. H. Apte, P. L. Groves, K. Klein, J. S. McCarthy, D. L. Doolan, Reduced plasmodium parasite burden associates with CD38⁺ CD4⁺ T cells displaying cytolytic potential and impaired IFN- γ production. *PLoS Pathog.* **12**, e1005839 (2016).
51. V. S. Patil, A. Madrigal, B. J. Schmiedel, J. Clarke, P. O'Rourke, A. D. de Silva, E. Harris, B. Peters, G. Seumois, D. Weiskopf, A. Sette, P. Vijayanand, Precursors of human CD4⁺ cytotoxic T lymphocytes identified by single-cell transcriptome analysis. *Sci. Immunol.* **3**, ean8664 (2018).
52. A. Takeuchi, S. Badr Mel, K. Miyauchi, C. Ishihara, R. Onishi, Z. Guo, Y. Sasaki, H. Ike, A. Takumi, N. M. Tsuji, Y. Murakami, T. Kataki, M. Kubo, T. Saito, CRTAM determines the CD4⁺ cytotoxic T lymphocyte lineage. *J. Exp. Med.* **213**, 123–138 (2016).
53. D. Weiskopf, D. J. Bangs, J. Sidney, R. V. Kolla, A. D. De Silva, A. M. de Silva, S. Crotty, B. Peters, A. Sette, Dengue virus infection elicits highly polarized CX3CR1⁺ cytotoxic CD4⁺ T cells associated with protective immunity. *Proc. Natl. Acad. Sci. U.S.A.* **112**, E4256–E4263 (2015).
54. D. Yang, Z. Tian, M. Zhang, W. Yang, J. Tang, Y. Wu, B. Ni, NKG2D⁺CD4⁺ T cells kill regulatory T cells in a NKG2D-NKG2D ligand-dependent manner in systemic lupus erythematosus. *Sci. Rep.* **7**, 1288 (2017).
55. D. Hirschhorn-Cymerman, S. Budhu, S. Kitano, C. Liu, F. Zhao, H. Zhong, A. M. Lesokhin, F. Avogadri-Connors, J. Yuan, Y. Li, A. N. Houghton, T. Merghoub, J. D. Wolchok, Induction of tumoricidal function in CD4⁺ T cells is associated with concomitant memory and terminally differentiated phenotype. *J. Exp. Med.* **209**, 2113–2126 (2012).
56. Y. Serroukh, C. Gu-Trantien, B. Hooshdar Kashani, M. Defrance, T. P. Vu Manh, A. Azouz, A. Detavernier, A. Hoyois, J. Das, M. Bizet, E. Pollet, T. Tabbuso, E. Calonne, K. van Gisbergen, M. Dalod, F. Fuks, S. Goriely, A. Marchant, The transcription factors Runx3 and ThPOK cross-regulate acquisition of cytotoxic function by human Th1 lymphocytes. *eLife* **7**, e30496 (2018).
57. R. Li, X. Chen, Y. You, X. Wang, Y. Liu, Q. Hu, W. Yan, Comprehensive portrait of recurrent glioblastoma multiforme in molecular and clinical characteristics. *Oncotarget* **6**, 30968–30974 (2015).
58. M. Stavrou, P. Philip, C. Traynor-White, C. G. Davis, S. Onuoha, S. Cordoba, S. Thomas, M. Pule, A rapamycin-activated caspase 9-based suicide gene. *Mol. Ther.* **26**, 1266–1276 (2018).
59. F. Akter, B. Simon, N. L. de Boer, N. Redjal, H. Wakimoto, K. Shah, Pre-clinical tumor models of primary brain tumors: Challenges and opportunities. *Biochim. Biophys. Acta Rev. Cancer* **1875**, 188458 (2021).
60. I. Simeonova, E. Huillard, In vivo models of brain tumors: roles of genetically engineered mouse models in understanding tumor biology and use in preclinical studies. *Cell. Mol. Life Sci.* **71**, 4007–4026 (2014).
61. S. Hervas-Stubbs, J. L. Perez-Gracia, A. Rouzaut, M. F. Sanmamed, A. Le Bon, I. Melero, Direct effects of type I interferons on cells of the immune system. *Clin. Cancer Res.* **17**, 2619–2627 (2011).
62. R. F. V. Medrano, A. Hunger, S. A. Mendonca, J. A. M. Barbutto, B. E. Strauss, Immunomodulatory and antitumor effects of type I interferons and their application in cancer therapy. *Oncotarget* **8**, 71249–71284 (2017).
63. S. H. Choi, D. W. Stuckey, S. Pignatta, C. Reinshagen, J. K. Khalsa, N. Roozendaal, J. Martinez-Quintanilla, K. Tamura, E. Keles, K. Shah, Tumor resection recruits effector T cells and boosts therapeutic efficacy of encapsulated stem cells expressing IFN β in glioblastomas. *Clin. Cancer Res.* **23**, 7047–7058 (2017).
64. C. Koba, M. Haruta, Y. Matsunaga, K. Matsumura, E. Haga, Y. Sasaki, T. Ikeda, K. Takamatsu, Y. Nishimura, S. Senju, Therapeutic effect of human iPSC-cell-derived myeloid cells expressing IFN- β against peritoneally disseminated cancer in xenograft models. *PLOS ONE* **8**, e67567 (2013).
65. S. A. Qezada, T. R. Simpson, K. S. Peggs, T. Merghoub, J. Vider, X. Fan, R. Blasberg, H. Yagita, P. Muranski, P. A. Antony, N. P. Restifo, J. P. Allison, Tumor-reactive CD4⁺ T cells develop cytotoxic activity and eradicate large established melanoma after transfer into lymphopenic hosts. *J. Exp. Med.* **207**, 637–650 (2010).
66. Y. Xie, A. Akpınarlı, C. Maris, E. L. Hipkiss, M. Lane, E. K. Kwon, P. Muranski, N. P. Restifo, P. A. Antony, Naive tumor-specific CD4⁺ T cells differentiated in vivo eradicate established melanoma. *J. Exp. Med.* **207**, 651–667 (2010).
67. Y. Kim, E. Kim, Q. Wu, O. Guryanova, M. Hitomi, J. D. Lathia, D. Serwanski, A. E. Sloan, R. J. Weil, J. Lee, A. Nishiyama, S. Bao, A. B. Hjelmeland, J. N. Rich, Platelet-derived growth factor receptors differentially inform intertumoral and intratumoral heterogeneity. *Genes Dev.* **26**, 1247–1262 (2012).
68. C. He, S. C. Medley, J. Kim, C. Sun, H. R. Kwon, H. Sakashita, Y. Pincu, L. Yao, D. Eppard, B. Dai, W. L. Berry, T. M. Griffin, L. E. Olson, STAT1 modulates tissue wasting or overgrowth downstream from PDGFR β . *Genes Dev.* **31**, 1666–1678 (2017).
69. F. Ciceri, C. Bonini, S. Marktel, E. Zappone, P. Servida, M. Bernardi, A. Pescarollo, A. Bondanza, R. Peccatori, S. Rossini, Z. Magnani, M. Salomoni, C. Benati, M. Ponzoni, L. Callegaro, P. Corradini, M. Bregni, C. Traversari, C. Bordignon, Antitumor effects of HSV-TK-engineered donor lymphocytes after allogeneic stem-cell transplantation. *Blood* **109**, 4698–4707 (2007).
70. F. Ciceri, C. Bonini, M. T. Stanghellini, A. Bondanza, C. Traversari, M. Salomoni, L. Turchetto, S. Colombi, M. Bernardi, J. Peccatori, A. Pescarollo, P. Servida, Z. Magnani, S. K. Perna, V. Valtolina, F. Crippa, L. Callegaro, E. Spoldi, R. Crocchiolo, K. Fleischhauer, M. Ponzoni, L. Vago, S. Rossini, A. Santoro, E. Todisco, J. Apperley, E. Olavarria, S. Slavin, E. M. Weissinger, A. Ganser, M. Stadler, E. Yannaki, A. Fassas, A. Anagnostopoulos, M. Bregni, C. G. Stampino, P. Bruzzi, C. Bordignon, Infusion of suicide-gene-engineered donor lymphocytes after family haploidentical haemopoietic stem-cell transplantation for leukaemia (the TK007 trial): A non-randomised phase I-II study. *Lancet Oncol.* **10**, 489–500 (2009).
71. K. Shah, S. Hingtgen, R. Kasmieh, J. L. Figueiredo, E. Garcia-Garcia, A. Martinez-Serrano, X. Breakefield, R. Weissleder, Bimodal viral vectors and in vivo imaging reveal the fate of human neural stem cells in experimental glioma model. *J. Neurosci.* **28**, 4406–4413 (2008).
72. F. A. Ran, P. D. Hsu, J. Wright, V. Agarwala, D. A. Scott, F. Zhang, Genome engineering using the CRISPR-Cas9 system. *Nat. Protoc.* **8**, 2281–2308 (2013).
73. N. E. Sanjana, O. Shalem, F. Zhang, Improved vectors and genome-wide libraries for CRISPR screening. *Nat. Methods* **11**, 783–784 (2014).
74. T. Wang, J. J. Wei, D. M. Sabatini, E. S. Lander, Genetic screens in human cells using the CRISPR-Cas9 system. *Science* **343**, 80–84 (2014).
75. W. M. Strauss, Preparation of genomic DNA from mammalian tissue. *Curr. Protoc. Mol. Biol.* **Chapter 2**, Unit2.2 (2001).
76. K. S. Chen, L. Harris, J. W. C. Lim, T. J. Harvey, M. Piper, R. M. Gronostajski, L. J. Richards, J. Bunt, Differential neuronal and glial expression of nuclear factor I proteins in the cerebral cortex of adult mice. *J. Comp. Neurol.* **525**, 2465–2483 (2017).
77. C. McQuin, A. Goodman, V. Chernyshev, B. A. Kametsky, B. A. Cimini, K. W. Karhohs, M. Doan, L. Ding, S. M. Rafelski, D. Thirstrup, W. Wiegand, S. Singh, T. Becker, J. C. Caicedo, A. E. Carpenter, CellProfiler 3.0: Next-generation image processing for biology. *PLOS Biol.* **16**, e2005970 (2018).
78. D. Kim, B. Langmead, S. L. Salzberg, HISAT: A fast spliced aligner with low memory requirements. *Nat. Methods* **12**, 357–360 (2015).

Acknowledgments: We would like to thank I. Verma for providing the CT2A cell line. We would like to thank S. Lawler for providing GL261 cell line and D. Fisher for providing B16 cell line. All schematics have been created for this manuscript using BioRender with a license to use the illustrations (K.S.). **Funding:** This work was supported by NIH grant R01-NS121096 to K.S. **Author contributions:** Conceptualization of this work was performed by K.S. The methodology for this work was devised by K.-S.C., C.R., T.A.V.S., F.R., P.B., N.C.M., H.W., and K.S. Experimental work was performed by K.-S.C., C.R., T.A.V.S., F.R., N.C.M., and B.S. The in vivo mouse experiments were performed by K.-S.C., C.R., and P.B. The project administration was managed by K.-S.C. and K.S. The project was supervised by K.-S.C., C.R., and K.S. The original draft of this manuscript was written by K.-S.C. and K.S. Reviewing and editing of this manuscript was performed by K.-S.C., C.R., T.A.V.S., F.R., R.A., D.A.R., H.W., and K.S. Funding was acquired by K.S. **Competing interests:** K.S. owns equity in and is a member of the Board of Directors of AMASA Therapeutics, a company developing stem cell-based therapies for cancer. K.S.'s interests were reviewed and are managed by Brigham and Women's Hospital and Mass General Brigham in accordance with their conflict of interest policies. The other authors declare that they have no competing interests. **Data and materials availability:** All data are available in the paper or the Supplementary Materials. The RNA-seq data generated and analyzed in this manuscript can be accessed at the Gene Expression Omnibus under accession number GSE217253. All cell lines and plasmids used in this study will be made available to the scientific community by contacting the corresponding author and completion of a material transfer agreement.

Submitted 5 February 2022
Resubmitted 29 August 2022
Accepted 7 December 2022

Published 4 January 2023
10.1126/scitranslmed.abo4778

Downloaded from <https://www.science.org> at Air Force Medical University on January 04, 2023

Bifunctional cancer cell–based vaccine concomitantly drives direct tumor killing and antitumor immunity

Kok-Siong ChenClemens ReinshagenThijs A. Van SchaikFilippo RossignoliPaulo BorgesNatalia Claire MendoncaReza AbdiBrennan SimonDavid A. ReardonHiroaki WakimotoKhalid Shah

Sci. Transl. Med., 15 (677), eabo4778. • DOI: 10.1126/scitranslmed.abo4778

View the article online

<https://www.science.org/doi/10.1126/scitranslmed.abo4778>

Permissions

<https://www.science.org/help/reprints-and-permissions>